AD-A058 985 EFRATOM SYSTEMS CORP IRVINE CA F/G 14/2
AN INVESTIGATION OF THE TECHNICAL FEASIBILITY OF USING PULSED O--ETC(U)
AUG 78 T C ENGLISH, E JECHART, T M KWON N00014-77-C-0646
UNCLASSIFIED NL

END
DATE FILMED
11-78
DDC

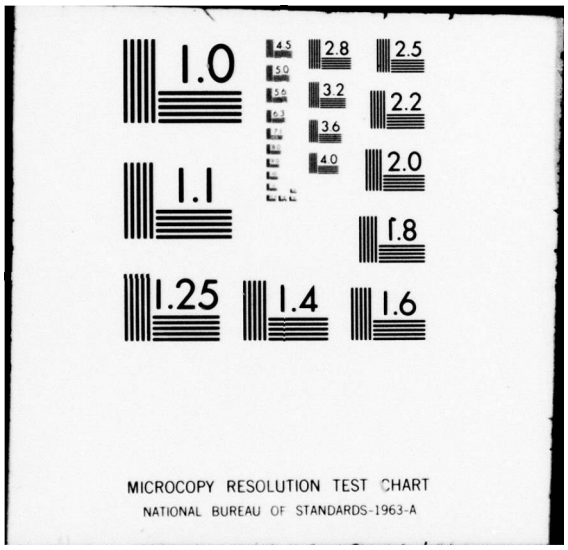
1.0
1.1
1.25
1.4
1.6
2.8
3.2
3.6
4.0
2.5
2.2
2.0
1.8
MICROCOPY RESOLUTION TEST CHART
NATIONAL BUREAU OF STANDARDS-1963-A

LEVEL II

(12)

(15) Report N00014-77-C-0646-001

EFRATOM

(6) AN INVESTIGATION OF THE TECHNICAL FEASIBILITY OF USING PULSED OPTICAL PUMPING TO ELIMINATE THE LIGHT SHIFT AND TO IMPROVE THE LONG-TERM STABILITY OF PASSIVE RUBIDIUM FREQUENCY STANDARDS.

(10) Thomas C. English, Ernst Jechart and T. M. Kwon
Efratom Systems Corporation
18851 Bardeen Avenue
Irvine, California 92715

410856

(11) 31 August 1978

(12) 86 p.

(9) Annual Summary Report, for Period 1 September 1977 to 31 August 1978

Distribution Unlimited

DDC RECEIVED SEP 22 1978 E

Prepared for

OFFICE OF NAVAL RESEARCH
Physics Program Office
Arlington, Virginia 22217

410856

Unclassified

SECURITY CLASSIFICATION OF THIS PAGE *(When Data Entered)*

REPORT DOCUMENTATION PAGE		READ INSTRUCTIONS BEFORE COMPLETING FORM
1. REPORT NUMBER N00014-77-C-0646-001	2. GOVT ACCESSION NO.	3. RECIPIENT'S CATALOG NUMBER
4. TITLE *(and Subtitle)* AN INVESTIGATION OF THE TECHNICAL FEASIBILITY OF USING PULSED OPTICAL PUMPING TO ELIMINATE THE LIGHT SHIFT AND IMPROVE THE LONG-TERM STABILITY OF PASSIVE RUBIDIUM FREQUENCY STANDARDS		5. TYPE OF REPORT & PERIOD COVERED Annual Summary Report 1 Sep 77 to 31 Aug 78 6. PERFORMING ORG. REPORT NUMBER
7. AUTHOR(s) Thomas C. English, Ernst Jechart and T.M. Kwon		8. CONTRACT OR GRANT NUMBER(s) Contract No. N00014-77-C-0646
9. PERFORMING ORGANIZATION NAME AND ADDRESS Efratom Systems Corporation 18851 Bardeen Avenue Irvine, California 92715		10. PROGRAM ELEMENT, PROJECT, TASK AREA & WORK UNIT NUMBERS Project Element and ID No. 121103
11. CONTROLLING OFFICE NAME AND ADDRESS Office of Naval Research Physics Program Office Arlington, Virginia 22217		12. REPORT DATE 31 August 1978 13. NUMBER OF PAGES 83
14. MONITORING AGENCY NAME & ADDRESS *(if different from Controlling Office)*		15. SECURITY CLASS. *(of this report)* Unclassified 15a. DECLASSIFICATION/DOWNGRADING SCHEDULE

16. DISTRIBUTION STATEMENT *(of this Report)*

Approved for public release; distribution unlimited.

17. DISTRIBUTION STATEMENT *(of the abstract entered in Block 20, if different from Report)*

18. SUPPLEMENTARY NOTES

19. KEY WORDS *(Continue on reverse side if necessary and identify by block number)*

atomic frequency standard, optical pumping, rubidium, alkali metal, relaxation time, magnetic resonance, light shift

20. ABSTRACT *(Continue on reverse side if necessary and identify by block number)*

A pulsed optical rubidium frequency standard has been constructed with the intent of investigating long-term frequency stability in the absence of light shifts. The short-term frequency stability of this device has been measured and found to be $\sigma_y = 2 \times 10^{-11} \tau^{-\frac{1}{2}}$ for τ = 1 to 100 sec. Measurements of the long-term frequency stability of this →

tau

next pg

DD FORM 1 JAN 73 1473 EDITION OF 1 NOV 65 IS OBSOLETE S/N 0102-LF-014-6601

Unclassified

SECURITY CLASSIFICATION OF THIS PAGE *(When Data Entered)*

Sigma sub Y

time to the -1/2 power (sq. rt. tau)

20. ABSTRACT (continued).

device (24 hour averaging time) show that σ_y is of order parts in 10^{12}, or better.

Various systematic effects have been investigated. These include frequency shifts that are produced by changes in the intensity of the pumping light, and by changes in the pulse parameters. Evidence is presented that shows that the former effect, which is small, does not behave like a true light shift. This pseudo light-shift is thought to be related to the "position-shift effect" of Risley and Busca. Means for reducing (or eliminating) it are suggested.

A simple theoretical model is presented that provides a conceptual picture of certain aspects of device operation. Semi-quantitative agreement between theory and experiment is obtained. In addition, a new method for measuring relaxation times in rubidium vapor devices is described.

TABLE OF CONTENTS

INTRODUCTION

Background and Motivation

The need for improvements in the state-of-the-art of compact, lightweight, low power, highly stable atomic frequency standards is exemplified by programs such as that for the NAVSTAR Global Positioning System (GPS).[1] The needs of the GPS program have resulted in efforts to advance the state-of -the-art, especially for hydrogen storage and cesium beam devices. These needs include size, weight, and power reductions and a fairly stringent long-term stability requirement (1×10^{-13} fractional frequency stability over periods of approximately one to twelve days for phase II of GPS). Requirements in future programs of this type can be expected to be even more demanding as the overall state-of-the-art of military technology moves forward.

Only three types of frequency standards appear to have been seriously considered for the GPS program: cesium beam, hydrogen, and rubidium gas cell devices. While the cesium and hydrogen devices have very good long-term stability, they tend to be bulky, heavy, and to exhibit moderate to high power consumption. Rubidium devices, on the other hand, can be made very compact, lightweight, and with low power requirements. (They also have excellent short-term stability.) As an example of the state-of-the-art in this respect, one commercial unit[2] has a volume of 1.1×10^{-3} m^3 (1.1 liters, about the size of a grapefruit), weighs 1.3 kg (2.9 lb), and uses only 13 W of power.

The long-term stability of commercial cesium devices is typically parts in 10^{13} and 10^{14} over periods of days to weeks, and parts in 10^{12} over much longer periods of time. Rubidium gas cell devices have generally been considered not to be competetive with cesium in this area, but recent data have shown that this is an over simplified point of view. For example, the stability of at least one commercial rubidium device[3] has been measured [4,5] and found to be parts in 10^{13} and 10^{14} over approximately 3×10^4 sec (8 hours). A high reliability version of this device, developed for use in phase I GPS satellites, has shown even better performance:[5] parts in 10^{13} and 10^{14} over 10^5 sec (30 hours).

To summarize, there is, at the present time, no single device among

atomic frequency standards that simutaneously provides state-of-the-art capability in all areas of interest, namely, low power consumption, small size and weight, good short-term frequency stability, and good long-term frequency stability. However, rubidium devices appear to come the closest to satisfying all of these requirements: it is much more likely that the long-term stability of rubidium devices can be significantly improved, than it is that the size and weight of cesium and hydrogen devices can be reduced to that of present day state-of-the-art rubidium devices.

Long-Term Stability of Rubidium Devices

There are at least three possible factors that have the potential of degrading the long-term stability of a rubidium gas cell device. They are: the so-called "light shift" effect, changes in buffer gas pressure, and the so-called "position-shift effect". The first two effects are well known and have been recognized as possible problem areas since the early days of optical pumping research.[6] The "position-shift effect" is a recent development[7] and results from inhomogeneities in the resonance cell, to be discussed later. The object of the work described in this report is to construct a rubidium gas cell device in which the light shift is eliminated to measure the resulting long-term stability of this device and then to study the effects of the remaining parameters on the long-term stability. It should also be mentioned that it appears possible with this approach to eliminate, or greatly reduce, the position-shift effect.

Pulsed Optical Pumping

The light shift effect can, in principle, be eliminated by using the technique of pulsed optical pumping. In this method, the pumping light and microwave radiation are alternately pulsed on and off at a rapid rate in such a way that the light and microwave radiations are never simultaneously present in the resonance cell, i.e., there is no temporal overlap between the light pulses and the microwave pulses. Since there is no pumping light present to shift the energies of the ground state hyperfine levels of the Rb atoms[8] when the microwave radiation is inducing the 0-0 hyperfine transition, there is no light shift.

Previous Work

It appears that the idea of using pulsed optical pumping first originated with Arditi.[9] In the original experiments,[10] it was demonstrated that there was no light shift to within the precision of the measurements (one part in 10^{10}), but the long-term stability was not investigated. To the best of our knowledge, the only work on pulsed optical pumping subsequent to that of reference 10 appears in the Russian literature. The Russian work, which is described below, has not really addressed the question of frequency stability using pulsed optical pumping; rather it has concentrated almost exclusively on the physics of the pulsed optical pumping process.

The paper by Yakobson[11] gives a theoretical treatment of pulsed pumping using a three-level model. The density matrix equations are solved using a Fourier series method to obtain approximate expressions for the susceptibility and line shape. This is done for three different detection schemes: (1) microwave detection of the oscillating magnetization of the Rb atoms (method used in reference 10); (2) optical detection using a weak cw auxilliary light source (second Rb lamp)in addition to the (pulsed) pumping light source; (3) optical detection using the pumping light (method used by us).

The first of four papers from Bazarov's group, reference 12, mostly contains experimental results for an apparatus that uses detection scheme (2), above. Data are presented for two different modes:cw microwave field, and pulsed microwave field. In both cases there is light-microwave overlap because the auxilliary (probe) light source is operated cw. As a result there is a light shift present. Graphs are given of light shift for values of other parameters. FM line shapes are also given. This work is of little interest in the present context.

The original work by Arditi and Carver[10] showed that it is possible to employ the time-domain equivalent of separated oscillating fields[13] to produce a "Ramsey pattern" for the line shape. This is done by using two temporally distinct microwave pulses during the dark time between successive light pulses. The advantage of this method is that it allows the line width to be made smaller than the natural line width (the latter being characterized by the relaxation time of the Rb atoms in the gas cell). In these original experiments, the Ramsey pattern was observed by microwave detection of

the oscillating magnetization of the Rb atoms. The second Russian paper,[14] from Bazarov's group, demonstrates experimentally that it is also possible to observe a Ramsey pattern using optical detection with a weak auxilliary (probe) light beam that is pulsed. In addition, this paper also gives a theoretical expression for the Ramsey line shape based on a simplified three-level model.

The most important Russian journal article is the third paper[15] from Bazarov's group which deals with light shifts in pulsed optical pumping. The pulsed pumping scheme that is considered in this paper is the same as that of the previous paper[14] from this group. In this third paper, the theory of the previous paper is developed in much greater detail, and with many of the previous restrictions removed; experimental results, including light shifts, are presented and interpreted using this theory. The significance of this paper is that the light shifts under consideration are occurring when there is no overlap between the light pulses and the applied microwave pulses (recall that the weak auxilliary light beam is also pulsed, as in reference 14). We believe that this effect is very small in our experiments, as is discussed later in this report.

The last Russian paper,[16] also from Bazarov's group, discusses (both theoretically and experimentally) the effect on the Ramsey pattern of more than two microwave pulses during the dark period of the pulsed pumping cycle.

It is clear from the Russian work that additional Russian work (not described above) has been done. Unfortunately this latter work has been published in that portion of the Russian literature that is inaccessible to us. However, judging from the references to this work (in the papers that are accessible to us), it is of minor importance compared to the work of Bazarov's group (references 12, 14-16).

Present Work

The scope of the work described in this report is shown in Figure 1. The design and construction of the apparatus is discussed in the next section. Subsequent sections of this report deal with the two other major aspects of this work: frequency stability measurements (see Figure 2) and fundamental device improvement (see Figure 3).

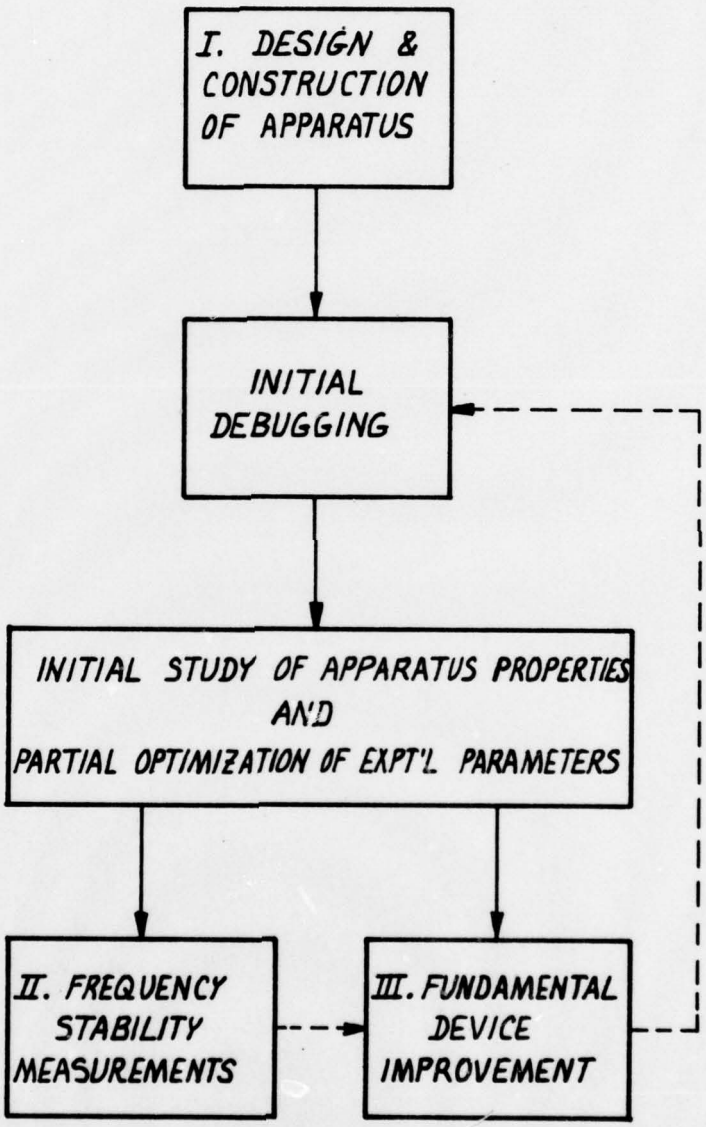

Figure 1. Scope of the work described in this report.

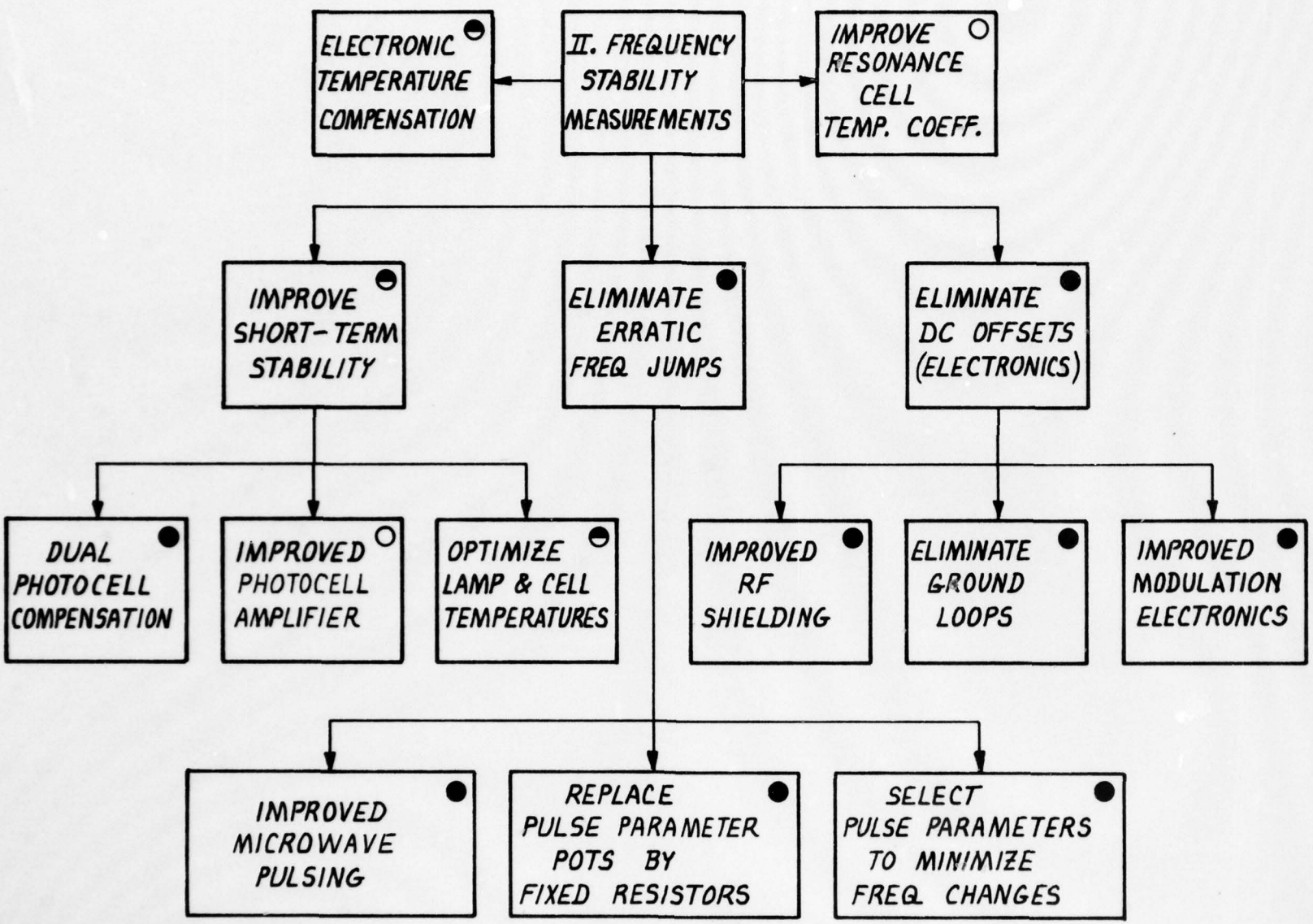

Figure 2. Flow chart for frequency stability measurements; ● = completed, ◒ = some work has been done, ○ = planned.

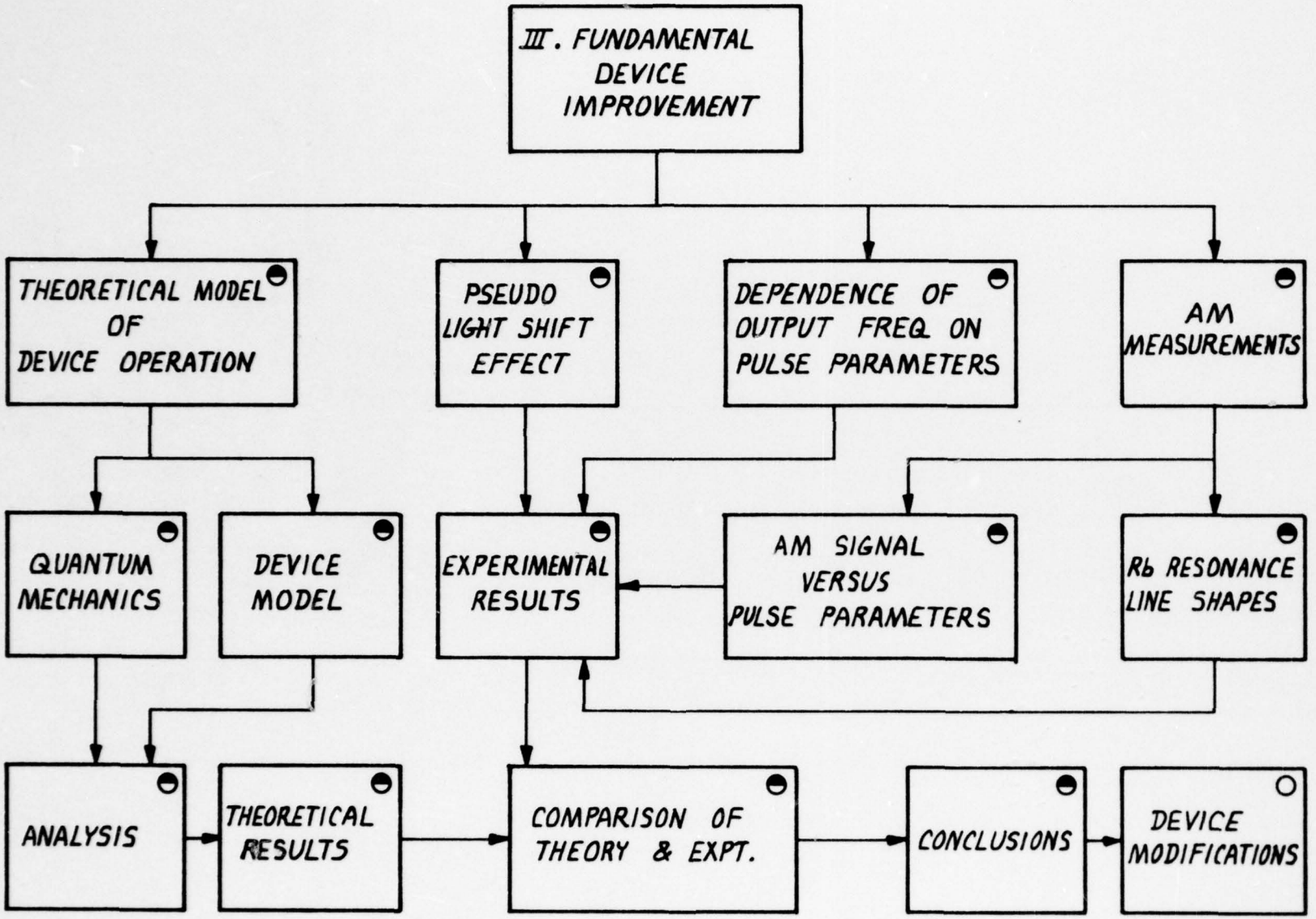

Figure 3. Flow chart for fundamental device improvement; ● = completed, ◓ = some work has been done, ○ = planned.

DESIGN AND CONSTRUCTION OF APPARATUS

Design Philosophy

In the original experiments of Arditi and Carver,[10] the oscillating magnetization of the Rb atoms was detected using a sensitive, microwave superheterodyne receiver. Besides adding considerable complexity to the electronic circuitry, this approach also requires use of a high Q microwave cavity for good S/N. This latter requirement has several disadvantages for practical devices: (1) small, low Q cavities, which are needed to reduce size and weight, cannot be used, and (2) the device becomes susceptible to cavity pulling.[17]

The work of Bazarov and coworkers has shown that it is possible to use optical detection instead of microwave detection. This eliminates the need for a superheterodyne receiver, but at the expense of adding a second (auxilliary) Rb lamp and its associated electronics. This is undesirable in a compact, lightweight, low power device because the Rb lamp consumes a significant fraction of the total power.

The design philosophy that has been adopted in the present work is that it is not profitable to conduct laboratory experiments using principles and methods that cannot subsequently be applied to the development of a compact, light weight, low power frequency standard. For this reason, we have chosen a substantially different approach to pulsed pumping than previous experimenters. This has been possible, at least in part, because of our prior expertise in developing and manufacturing small, light weight, and low power rubidium frequency standards exhibiting state-of-the-art performance.

Our approach has been to construct an experimental pulsed optical pumping apparatus using as a starting point the Efratom Model FRK miniature rubidium frequency standard[18] (hereafter referred to as the FRK). The physics package in this unit (which includes the Rb lamp and associated electronics) is approximately cylindrical in shape with a diameter of 0.057 m (2.25 in.) and a length of 0.10 m (4.0 in.). The small size is made possible mainly by the substitution of a TE_{111} microwave cavity for the more conventional but larger TE_{011} cavity, and by eliminating the need for a separate filter cell. The latter is accomplished by combining the filtering function with the resonance function in the resonance cell. This dual function cell is usually

referred to as an "integrated cell".

The pulsed optical pumping apparatus that we have constructed uses an unmodified FRK physics package. The Rb lamp operates on the plasma discharge principle using a 90 MHz driving source. The lamp is pulsed on and off by pulsing the dc supply voltage of the 90 MHz lamp driver.

In our experimental apparatus the Rb resonance is detected optically by observing the absorption of the pumping light. This eliminates the need for a sensitive microwave receiver and a high Q microwave cavity. Our detection scheme also eliminates the need for a second (auxilliary) Rb lamp. This is why it has been possible to use an unmodified FRK, miniature physics package.

The pulsing scheme for these experiments is shown in Figure 4. The lamp is pulsed on for a time T_ℓ. After the lamp is turned off, a time T_s elapses before the microwave pulse is pulsed on. The duration of the microwave pulse is T_μ. Following the end of the microwave pulse, is a period of time T_d' before the beginning of the next cycle. All times typically lie in the range of 0.1 to 10 msec. As can be seen from the figure, the dark time $T_d = T_\mu + T_d'$, and the cycle time $T_c = T_\ell + T_d$. So far, we have used only a single microwave pulse between successive light pulses. We could very easily obtain a Ramsey pattern by modifying our pulsing circuitry so that our single microwave pulse of Figure 4 would be replaced by two (or more) microwave pulses. We have chosen not to do this at the present time because of the added complexity that it introduces when interpreting the experimental results; moreover, it is not even certain that this could produce any improvement in device performance.

As can be seen from Figure 1 (and Figure 3), two parallel approaches have been employed. The first involves making frequency stability measurements, usually over periods of 4×10^4 sec (12 hours) to 2×10^5 sec (2½ days), and seeking to improve device stability by means that do not require a fundamental understanding of device operation. The second involves a fundamental investigation of device characteristics for the purpose of improving device operation as a frequency standard. In the first approach (device operating as a frequency standard) it is necessary to frequency modulate the atomic resonance (FM mode of operation). In the second approach it is desirable, in addition, to be able to amplitude modulate the atomic resonance (AM mode of operation) because this makes certain device para-

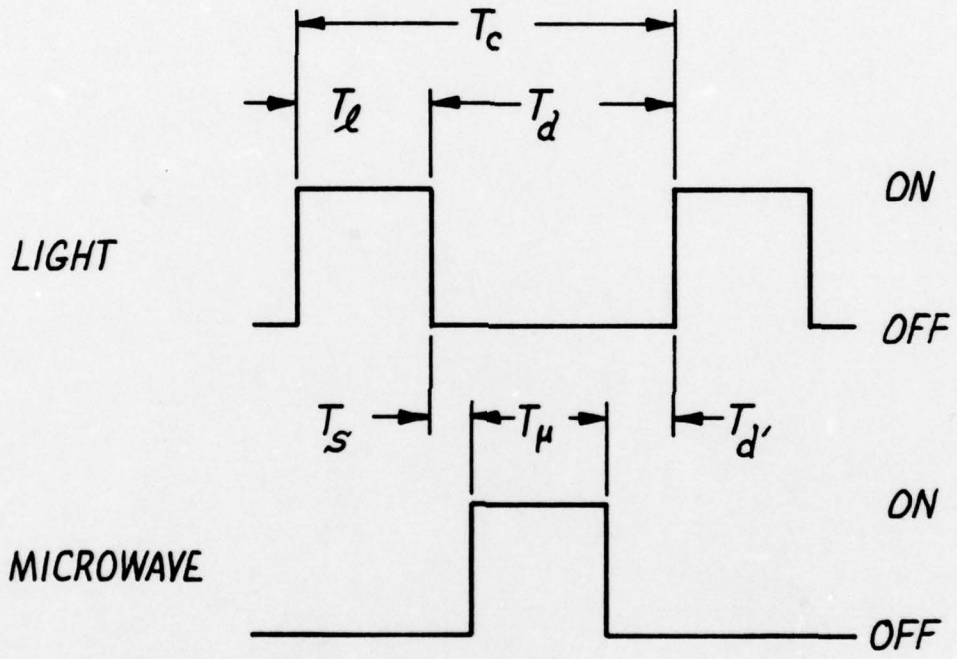

Figure 4. Pulsing scheme for work described in this report. Symbols are defined in the text.

meters accessible (e.g., atomic line shapes and relaxation times) that cannot be simply determined using the FM mode. For this reason, two different experimental configurations (AM and FM) have been used. Both are described below.

AM Configuration

Initial considerations involving relaxation times and resonance line widths indicated that the frequency of the pulsing cycle for optimum signal (AM or FM) would be of the order of several hundred hertz. The modulation frequency, i.e., the frequency for phase sensitive detection ("lock-in" frequency), appears as a small modulation of the amplitude of the light pulses reaching the photodetector. Since this modulation amounts to about 10^{-3} to 10^{-4} of the light pulse amplitude, it is imperative to be able to separate the signal component at the modulation frequency from the undesired component at the pulsing frequency. This can be done using analog filtering techniques if the modulation frequency differs appreciably from the pulsing frequency. For this reason, the modulation frequency was chosen to be 10 Hz.

Figure 5 is a diagram of the AM pulsed optical pumping apparatus. To expedite and simplify apparatus construction, electronic circuits and components which comprise the Model FRK, commercial rubidium frequency standard were used where possible. Even so, it was necessary to design and construct some of the blocks using discrete components and integrated circuits. These blocks included the pulsing electronics (see Figure 6 for details), the 10 Hz signal conditioner and amplifier (see Figure 7 for details), and the 10 Hz modulation oscillator. In addition, it was necessary to build a 5 MHz, pulsed rf switch and buffer amplifier. This device is included in the microwave synthesizer block in Figures 5 and 8.

The AM operation is best explained by reference to Figure 5. If the device is operated cw, the Rb lamp runs continuously and the 6.8 GHz microwave radiation is effectively switched on and off (square wave) at a 10 Hz rate ("lock-in" frequency). When the 6.8 GHz is tuned to the center of the Rb hyperfine resonance ($F=1, M_F = 0 \longleftrightarrow F=2, M_F = 0$), the light from the Rb lamp that passes through the Rb resonance cell, and is incident on the photodetector, is modulated at 10 Hz. This 10 Hz component is amplified,

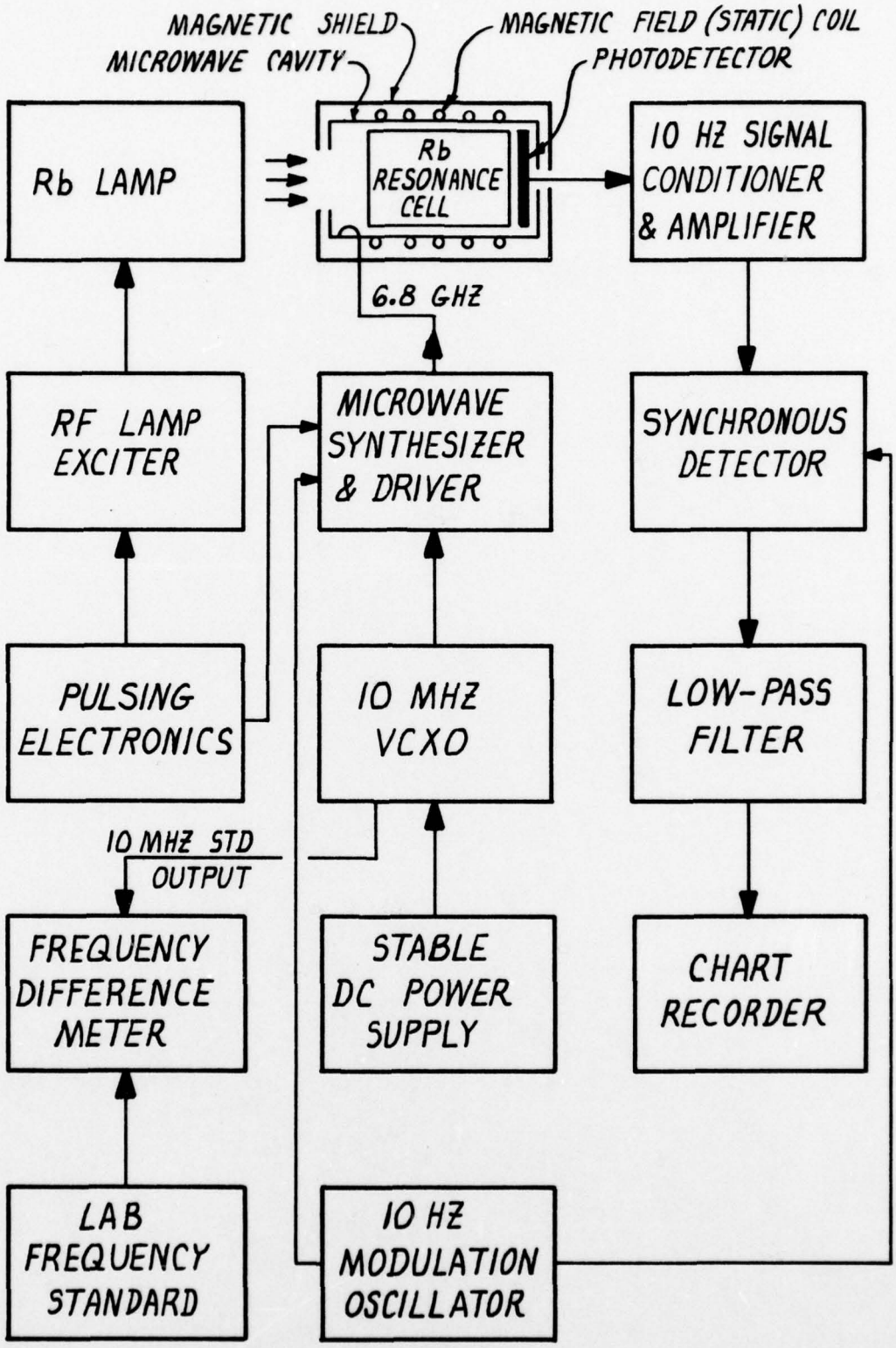

Figure 5. Block diagram of AM pulsed optical pumping apparatus.

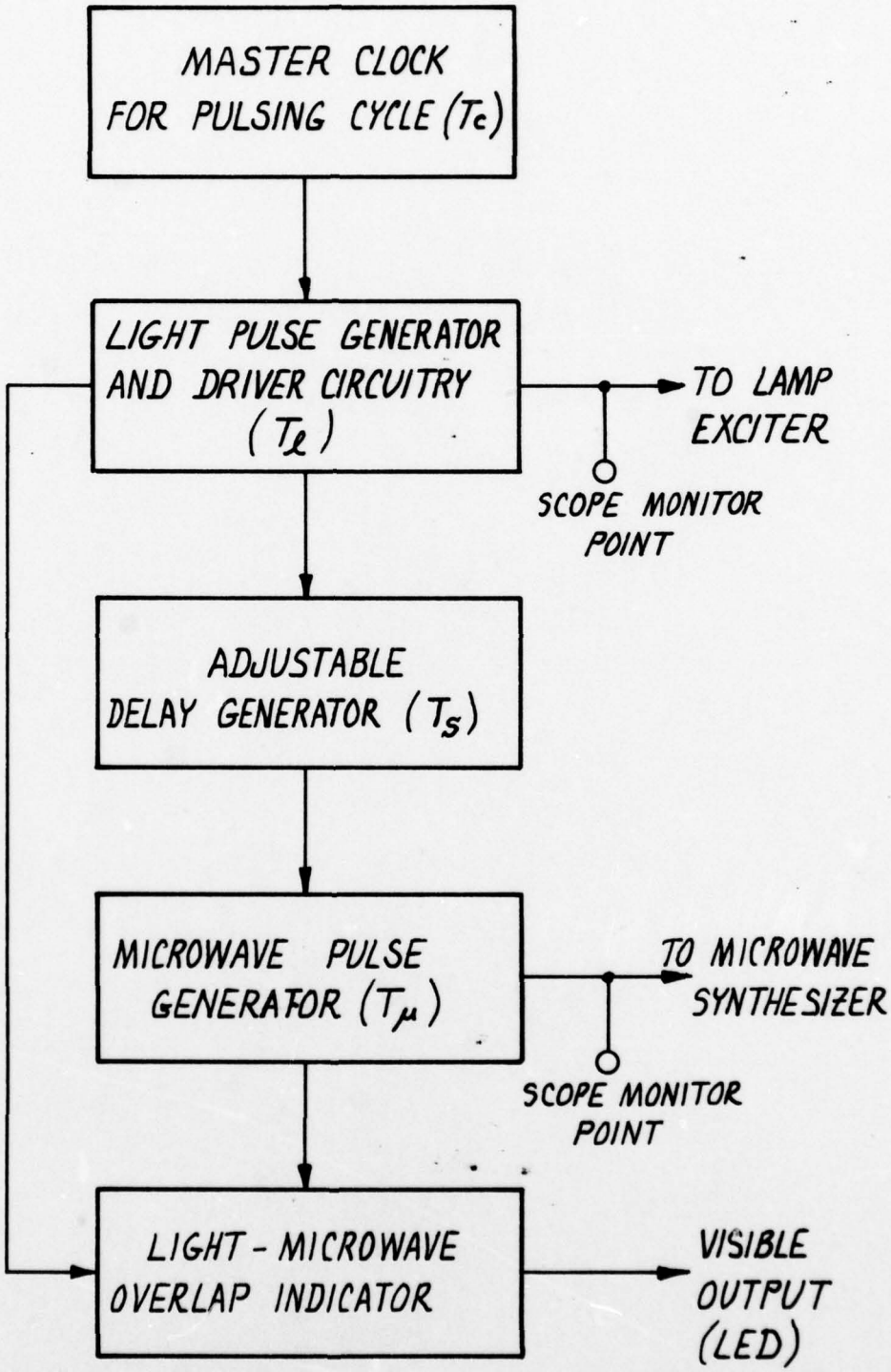

Figure 6. Block diagram of pulsing electronics.

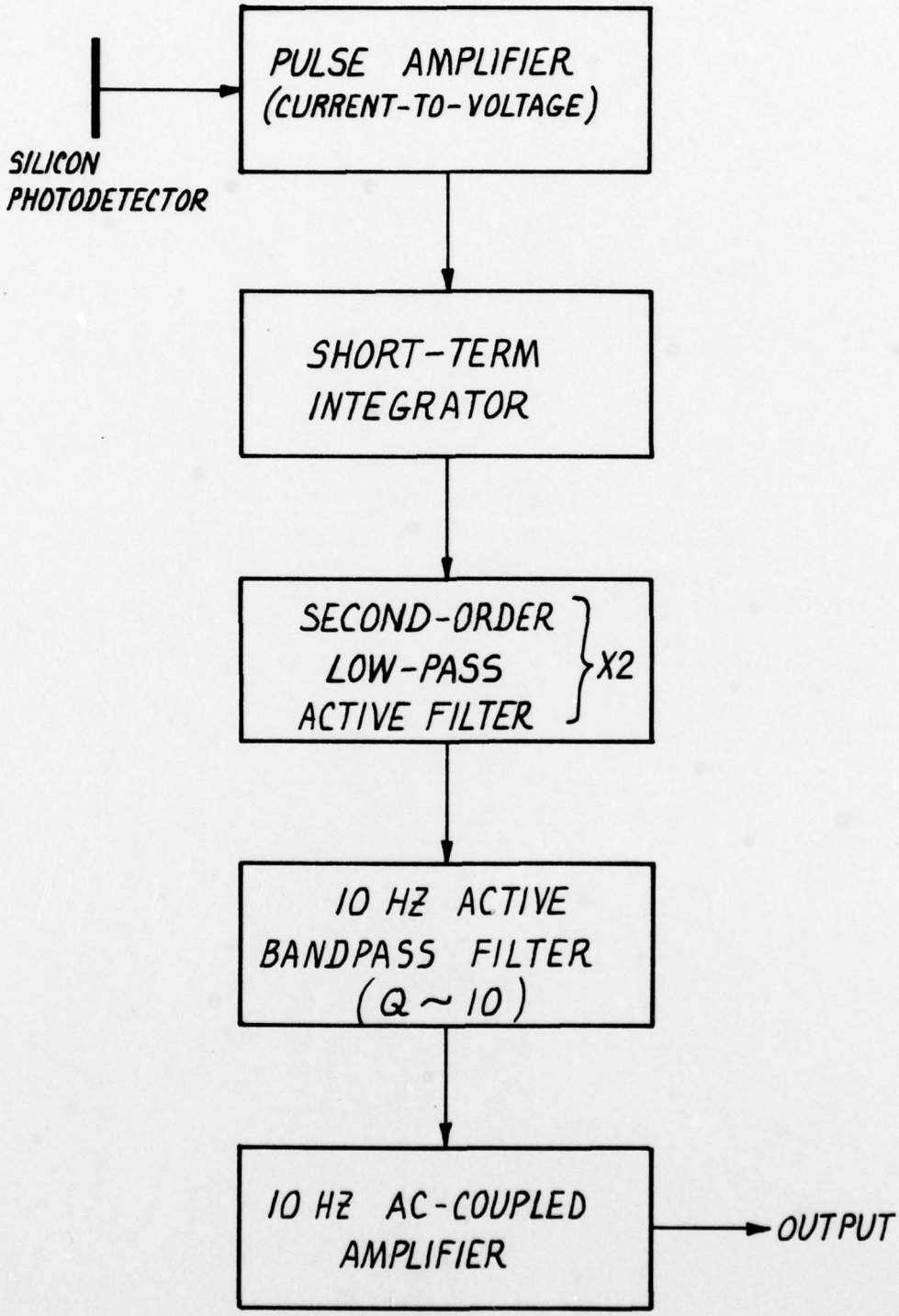

Figure 7. Block diagram of 10 Hz signal conditioner and amplifier.

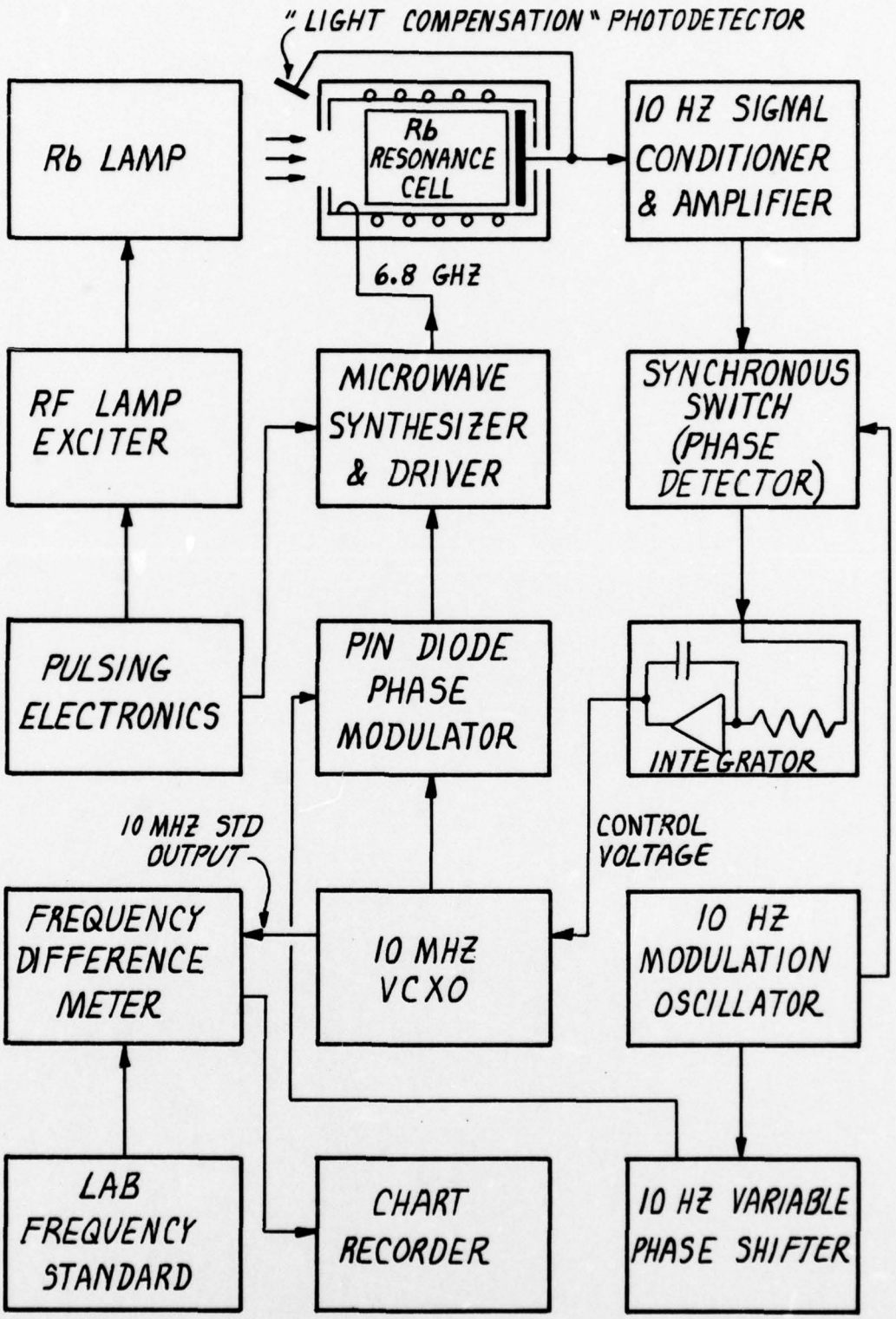

Figure 8. Block diagram of FM pulsed optical pumping apparatus connected as a frequency standard.

synchronously detected, filtered, and displayed on a chart recorder. The output from the VCXO is multiplied (by 684) and synthesized to obtain the 6.8 GHz. The frequency of the 6.8 GHz is controlled by a stable dc power supply that determines the frequency of the 10 MHz voltage controlled crystal oscillator (VCXO).

Normally, the device is not operated cw; the light and microwave radiation are pulsed using the scheme shown in Figure 4. The AM operation is then modified as follows. The Rb lamp is pulsed on and off at the pulsing frequency, and is unaffected by the 10 Hz modulation. During half of the 10 Hz modulation cycle the microwave radiation is turned off. During the other half of the 10 Hz cycle, the microwave radiation is pulsed on and off at the pulsing frequency (according to Figure 4) so that there is no light-microwave overlap. Since the pulsing frequency is of order 300 Hz, there are approximately 15 cycles of light pulsing that occur during each half of the modulation cycle. It should be noted that the pulsing frequency and the modulation frequency are derived from independent oscillators so that the pulsing is asynchronous with the 10 Hz modulation.

In practice it is undesirable to pulse the 6.8 GHz microwave radiation completely on and off because of potential rf pickup problems. Instead, the microwave radiation is effectively turned off by shifting its frequency by ~ 5 MHz. This method works because the 5 MHz shift is much greater than the width of the atomic resonance (~ several kHz in the worst case). In Figure 5 (and also in Figure 8), the 6.834... GHz is synthesized by multiplying the VCXO frequency by six to obtain 60 MHz. The 60 MHz is then multiplied by 114 and mixed with 5.3125 MHz in a step recovery diode to yield 6.834... GHz. In our scheme of pulsing, the 5.3125 MHz is gated on and off using a pulsed rf switch and buffer amplifier.

The apparatus of Figure 5 has been used to measure changes in AM signal as a function of device parameters. For most measurements of this type, the VCXO is tuned to a frequency that corresonds to the Rb resonance frequency, and other parameters (T_ℓ, T_μ, T_d, etc) are then varied (one at a time). If the VCXO frequency is varied while all other parameters are held fixed, one obtains the atomic line shape for those experimental conditions.

To avoid possible confusion, it should be kept in mind that AM operation is always open loop; i.e., servo-type (or feedback) operation is not possible using the AM configuration shown in Figure 5.

FM Configuration

The FM configuration shown in Figure 8 allows the pulsed pumping apparatus to be operated as a frequency standard. The FM method, as used here, consists of sinusoidally sweeping the frequency of the 6.8 GHz radiation back and forth across the Rb resonance at a 10 Hz rate. This produces a 10 Hz modulation of the light pulses reaching the photodetector which, when amplified and synchronously detected, gives a dc output voltage as shown schematically in Figure 9. The physics package, and this portion of the electronics, therefore function as a frequency discriminator that gives a negative (positive) output voltage when the frequency of the 6.8 GHz microwave radiation lies above (below) the Rb resonant frequency. If this error signal is fed back, and used to control the VCXO frequency, operation as a frequency standard results.

The FM configuration of Figure 8 differs from the AM configuration of Figure 5 in the following respects:

The 10 Hz modulation oscillator is no longer used to pulse the microwave radiation on and off (effectively). Instead, it is used to phase modulate the 10 MHz output of the VCXO. This produces frequency modulation of the 6.8 GHz. The advantage of phase modulation over frequency modulation is that the frequency of the VCXO remains spectrally pure (if <u>frequency</u> modulation of the 10 MHz at a 10 Hz rate were used, the VCXO frequency spectrum would contain sidebands spaced at 10 Hz intervals). Phase modulation is accomplished using a PIN diode phase modulator. This device has the advantage of linearity for phase deviations that would produce nonlinearity if a varactor diode phase modulator were used instead. The PIN diode acts as an electrically - controllable rf resistor and is used in a standard RC phase shifter configuration. The optimum value of the peak phase deviation at 10 MHz has been determined experimentally to be $\sim 3^{o}$. This corresponds to a peak frequency deviation at 6.8 GHz that is somewhat greater than the Rb resonance line width.

In addition to the phase modulator, a 10 Hz variable phase shifter was designed and built so that the 10 Hz signal could be phase shifted relative to the 10 Hz reference. This is required for the phase detection scheme used. The synchronous switch and integrator were taken from an FRK and modified for use here.

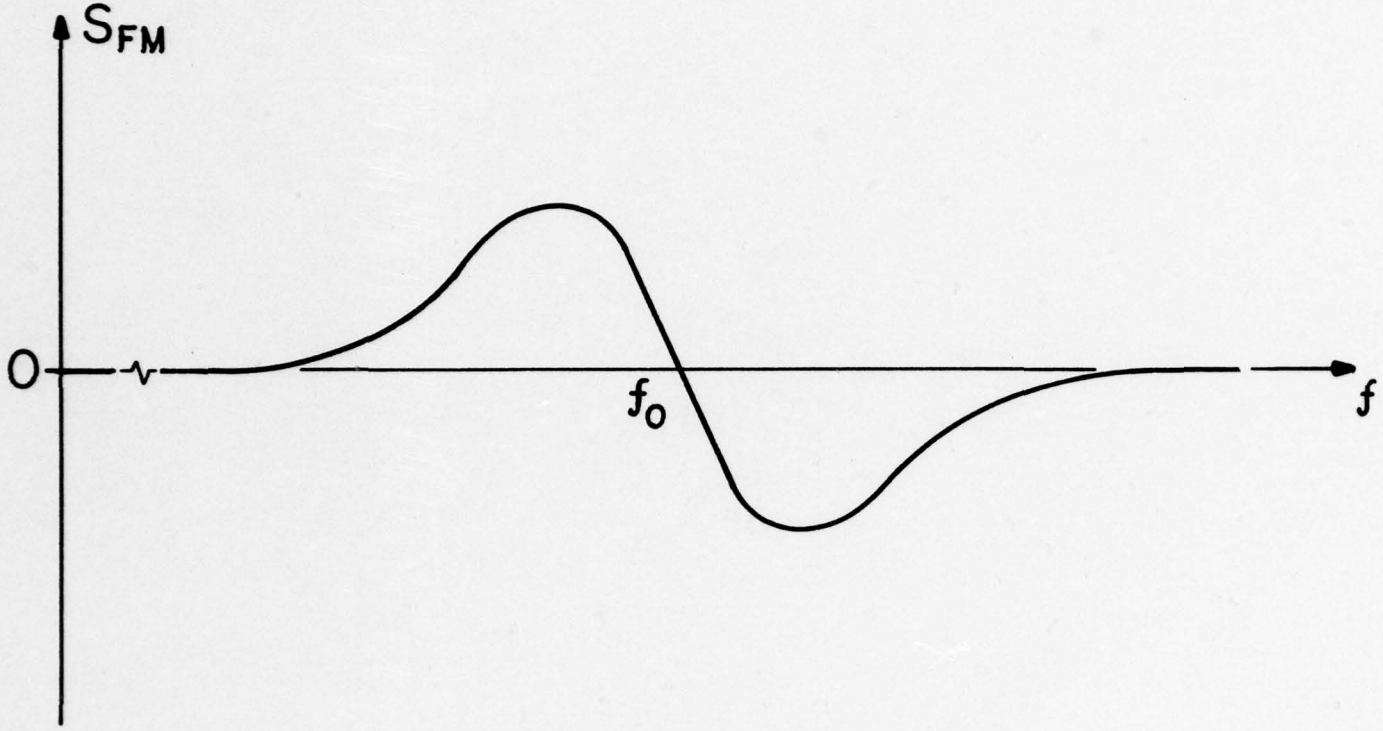

Figure 9. Schematic diagram of dc output of phase detector as a function of microwave frequency for FM configuration (Figure 8, with loop open). f_0 is the Rb resonance frequency, 6.834...GHz.

FREQUENCY STABILITY MEASUREMENTS

As mentioned previously, two parallel approaches have been used in this work. The first, which is discussed here, consists of making frequency stability measurements and seeking to improve device stability by means that do not require a fundamental understanding of device physics.

Methods of Measurement

Two methods of measuring frequency stability have been used in this work. In the first, the 10 MHz output of the VCXO is divided by two and fed to the input of a Tracor Model 527A frequency difference meter (FDM). The output of the Tracor is a dc voltage that is proportional to the difference between the VCXO frequency and that of a 5 MHz reference. The reference ("lab frequency standard" in Figures 5 and 8) is essentially an Efratom Model FRK-H rubidium frequency standard that has been specially selected and modified to provide superior performance and temperature stability. The dc output of the FDM is passed through an RC smoothing network and then displayed on a chart recorder.

The second method uses a custom-built TTL phase comparator. This device gives a dc output that is proportional to the phase difference between the VCXO frequency and the reference ("lab standard") frequency, modulo 2π.

The FDM is more convenient to use, but it is difficult to relate its output indication to the commonly accepted measure of frequency stability, the Allan variance.[19] Also, the RC time constant is limited to about 100 sec. On the other hand, the Allan variance can be determined for arbitrarily long averaging times from the phase comparator data.

Problems and Solutions

Figure 2 shows the problems that have been encountered in obtaining good frequency stability with the pulsed pumping apparatus, and the progress made in finding solutions.

Erratic Frequency Jumps

Considerable time was spent trying to eliminate spontaneous frequency jumps. Typically, these jumps were several parts in 10^{10} and would appear as a step function in frequency. This problem was particularly difficult to solve because it was due to several causes. Three methods of attack were utilized in solving this problem. The first was the improvement of the rf pulsing scheme. This was carried out by designing and building a 5.3 MHz buffer amplifier and pulsed rf switch. This circuit pulses the 5.3 MHz on and off to provide millisecond pulses of 5.3 MHz (with rise and fall times of $\leq$ 10 μsec) that are fed to the step recovery diode. The first stage is an emitter follower buffer that isolates the 5.3 MHz source from the rf switch. A PIN diode (HP 3080) rf switch follows this stage. The rf pulses from the PIN diode network are amplified and cleaned up using a tuned FET amplifier, and then passed into the final stage which is an emitter follower driver. The previous scheme for pulsing the 5.3 MHz was much simpler but the pulses were not clean, and the 5.3 MHz source was modulated at the pulsing frequency. The present scheme eliminates these problems.

The second method of attack was much simpler, but at least as effective. The pots used to adjust the pulsing parameters (T_ℓ, T_μ and T_c; see Figure 6) were replaced by fixed metal film resistors. This eliminated small jumps in the pulse parameters due to small changes in pot resistances. Related to this was the third method of attack, which involved selecting values of the pulse parameters to reduce the sensitivity of the output frequency to small changes in these parameters.

Since these measures have been instituted, frequency jumps have ceased to be a problem.

Dc Offsets

Dc offsets in the electronics, particularly when they occur in the signal channel between the photocell and the VCXO (see Figure 8), produce corresponding offsets in the output frequency. As an example of this, consider what happens when a dc offset is applied to the input of the integrator in Figure 8. This dc voltage causes the output voltage

of the integrator to begin changing. This, in turn, changes the VCXO frequency which detunes the 6.8 GHz from the Rb resonance frequency. This detuning generates a dc voltage at the output of the phase detector (in accordance with Figure 9) which tends to oppose the dc offset that was originally applied. The servo loop therefore seeks to adjust itself in such a way as to produce a null condition at the integrator input (net dc input offset = 0). Obviously, the only way that it can do this is to detune the VCXO (and therefore the 6.8 GHz) sufficiently to produce an error voltage at the input of the integrator that just cancels the original dc offset (the dc loop gain for our loop is $\sim 10^6$ so that finite gain effects are unimportant here). A detailed analysis[20] shows that the frequency offset is proportional to the dc offset, to the gain of the preceding electronics, and to the gain of the physics package (all suitably defined). The output frequency therefore becomes dependent on the gain of the electronics and the physics package which is clearly very undesirable since it cannot be assumed that these gains remain constant, especially over long periods of time.

Another difficulty occurs when the dc offset is due, for example, to rf pickup (mostly 60 MHz from the microwave synthesizer and the physics package, wherein is located the step recovery diode). One way this can occur is if there is partial rectification of the rf due to nonlinearity in the signal electronics. This type of dc offset is particularly troublesome because it is difficult to eliminate, and it is sensitive to the relative positions of circuits, wires and ground locations, all of which are subject to change. This effect was eliminated in our apparatus by improving the rf shielding, grounding, and decoupling. A significant effort was necessary to accomplish this.

A somewhat related problem is the presence of dc offsets due to ground loops, and inadequate power supply decoupling. With care, these problems can be essentially eliminated.

All of the offsets discussed so far can be easily detected by varying the gain of the electronics. On the basis of this type of measurement, it is estimated that dc offsets of the type discussed can be reduced to the extent that a 10% change in gain produces a frequency shift of less than 1×10^{-12}. (The actual shift may be much lower than

this; 1×10^{-12} is an upper limit imposed by the resolution of our measurements.)

Another possible source of dc offset is second-harmonic contamination of the 10 Hz modulation.[21,20] If this offset is constant there is no detrimental effect, but this cannot be taken for granted. When this offset is present, changes in the second-harmonic content of the modulation can produce output frequency shifts. Even if the amount of second harmonic does not change, output frequency shifts can still result from changes in the relative phases of signal and reference at the phase detector[20] due to the presence of second harmonic in the modulation.

Second-harmonic contamination was investigated in considerable detail. Since the problem is difficult to treat theoretically for large angle modulation (~ 10π at 6.8 GHz), a circuit was designed to inject known amounts of second harmonic into the 10 Hz modulation, so that the corresponding shifts in the 10 MHz output frequency could be observed. Using this method, it was found that the shift in the output frequency is proportional to the amplitude of the in-phase component (i.e., $\cos 2\omega_m t$ for $\cos \omega_m t$ modulation, where $\omega_m/2\pi$ = 10 Hz) of second harmonic. It was also verified (as expected from theoretical considerations) that the frequency offset is independent of the gain of the signal electronics, which makes it difficult to detect its presence. For cw operation of the frequency standard, an in-phase second-harmonic contamination of -23 dB produced a frequency offset of 1×10^{-9}. (The result for pulsed operation is not expected to be significantly different.)

Measurements were also made of the second-harmonic content of the 10 Hz analog signal used to drive the 10 MHz PIN diode phase modulator. To do this, a simple, low-frequency Fourier analyzer was constructed. An upper limit of -66 dB was established for the amount of second harmonic. If this amount of in-phase second harmonic contamination were present, the resultant frequency offset would be approximately 7×10^{-12}. It is likely that the actual offset is considerably less than this.

Even if the 10 Hz driving signal contains no 20 Hz component, it is still possible to generate a 20 Hz component in the modulation circuitry (due to possible nonlinearity of the modulator). Unfortunately

there appears to be no simple, direct way to investigate this possibility. An indirect method consists of observing the amount of out-of-phase first harmonic in the signal from the physics package (which is due to the out-of-phase component of second harmonic in the modulation) when the servo loop is closed and the VCXO is locked to the Rb resonance. We have done this for our apparatus and have found negligible out-of-phase first harmonic. This strongly suggests (but does not prove) that there is negligible second harmonic contamination of the modulation in our apparatus.

It should be mentioned that several modifications of the modulation circuitry were made prior to the above measurements. The 10 Hz analog PIN diode driver was redesigned to provide more distortion-free operation, and the 10 Hz amplitude and dc bias controls were made orthogonal. Most importantly, the PIN diode modulator itself was redesigned to use five PIN diodes (HP 3080) rather than a single diode. This allows the use of higher drive levels and reduces the susceptibility to noise and spurious signals.

To summarize, modifications of the modulation circuitry have been made that have resulted in improved operation. Measurements made on this improved circuitry, and on the apparatus as a whole, have indicated that dc offsets and frequency offsets due to second-harmonic contamination of the 10 Hz modulation are small, if they exist at all, and that degradation of frequency stability due to these effects is probably negligible.

Short-Term Stability (τ = 1 to 100 sec)

The signal-to-noise ratio of the apparatus determines the short-term frequency stability for averaging times greater than the attack time of the servo loop (~ 0.2 sec). It has been found that the signal in the pulsed mode is quite good: generally about 20% to 30% of that obtained in the cw mode. The noise, however, is significantly greater in the pulsed mode. This is not surprizing since the 10 Hz signal component is of the order of 10^{-3} of the amplitude of the pulses. If the light pulses exhibit spurious (noise) amplitude changes from pulse to pulse, or if there is light-pulse-width jitter, then the 10 Hz Fourier components will produce frequency noise. Clearly, changes in amplitude and pulse duration as

small as 10^{-5} have the potential of producing 10 Hz noise.

It has been found possible to reduce the 10 Hz noise by a factor of ~ 7 by using a "light compensation" scheme which employs two photodetectors. Besides the usual photodetector, a second one is placed in front of the Rb resonance cell, close to the Rb lamp (see Figure 8). The two detectors are connected so that their output pulses tend to cancel. Since only the usual photodetector receives the 10 Hz signal component, the 10 Hz signal is unchanged. This scheme greatly reduces the background signal. Using this method, one typically observes a peak-peak fractional frequency fluctuation of 1×10^{-11} with a 100 second time constant on the output of the FDM. This is very nearly equal to the fractional frequency fluctuation obtained in the cw mode for a 10 Hz modulation frequency. Additional measurements for 1 and 10 second time constants show that the fractional frequency stability is improving in proportion to $t^{-\frac{1}{2}}$ where t is the time constant. This shows that we are dealing with white frequency modulation noise,[19] as is usually the case for passive rubidium devices.

As noted previously, the FDM readings are not easily related (analytically) to the usual measure of frequency stability, which is the square root of the Allan variance (denoted by $\sigma_y(\tau)$ where τ is the averaging time). However, experience gained at Efratom with our commercial units has shown that $\sigma_y(\tau)$ for $\tau = t$ can be estimated quite reliably from FDM readings by dividing the FDM peak-peak fractional frequency fluctuations by six (dividing by five gives a more conservative result). Since our FDM readings for the pulsed pumping apparatus have the expected $t^{-\frac{1}{2}}$ dependence, this procedure should also be valid here. We therefore conclude that for our pulsed pumping frequency standard, the short-term stability is given by

$$\sigma_y(\tau) = 2 \times 10^{-11}\, \tau^{-\frac{1}{2}},\ 1 \leq \tau \leq 100 \text{ sec.} \qquad (1)$$

In particular, for $\tau = 100$ sec, $\sigma_y = 2 \times 10^{-12}$. This value is listed in Table 1 along with values of σ_y (100 sec) for other frequency standards. Note that the short-term stability of the pulsed pumping device is better than that of a commercial cesium beam, and comparable to commercial rubidiums.

TABLE 1. SHORT-TERM FREQUENCY STABILITY
OF SEVERAL FREQUENCY STANDARDS FOR A
100 SEC AVERAGING TIME

Frequency standard	Fractional frequency stability[a]
Pulsed optical pumping (present work)[b]	2×10^{-12}
Hewlett-Packard 5062C cesium beam[c]	7×10^{-12}
Efratom FRK-L rubidium[c]	3×10^{-12}
FRK-H rubidium[c]	1×10^{-12}
Oscilloquartz B-5400 high stability quartz[c]	1×10^{-12}
Efratom FRK-H rubidium, Serial No. 2610[d]	3×10^{-13}

[a]Square root of Allan variance, $\sigma_y(\tau)$, for τ = 100 sec.
[b]See text for explanation.
[c]Manufacturer's specification
[d]Data taken at Rockwell International, Autonetics Division, Anaheim, California, 17 Nov. 77. $\sigma_y(\tau = 100 \text{ sec}) = (2.95 \pm 0.26) \times 10^{-13}$ for FRK-H, S/N 2610 using HP 5065 reference, rounded to 3×10^{-13}.

Tests have been conducted to determine the sources of noise in the pulsed pumping apparatus. Open-loop noise measurements have been made, and the open-loop gains of the signal electronics and physics package have been determined as well. From these data it is a simple matter to calculate the contributions of the various noise sources to the observed $\sigma_y(\tau)$. It is found that the lamp is the major contributor. However, if there were no lamp noise, σ_y would improve by only a factor of two. As a check on this method, the total σ_y was calculated from the total open-loop noise and found to be $(\sigma_y)_{calc} = 1.6 \times 10^{-12}$. The value of σ_y measured with the servo loop closed is $(\sigma_y)_{meas} = 2 \times 10^{-12}$. (Both are for $\tau = 100$ sec.) The agreement lies within the experimental uncertainties.

The implication of the above result is that any effort to increase S/N ratio by more than a factor of two, must consider both lamp noise and amplifier noise. In fact, it appears possible to improve the S/N by any of several methods. One method is to improve the signal. Under certain conditions ^{87}Rb lamps can give larger signals then we presently obtain with the present lamp (that contains both isotopes of Rb). Optimization of lamp and cell temperatures (simultaneously with the pulsing parameters) could also yield greater signal. At the present time, systematic studies of this nature have not been carried out so that additional improvements are probably possible.

The other method of improving the S/N is to decrease the noise. It may be possible to reduce the lamp noise by proper choice of lamp operating conditions (tests have shown that the noise is not due to the pulsing electronics). Very little effort has been expended in this area. It also appears to be possible to reduce amplifier noise at 10 Hz by using a different op amp for the input stage of the photocell amplifier. We base this statement on some independent IR&D work that we have done using our commercial units.

In summary, we note that the presently measured short-term frequency stability of our pulsed pumping frequency standard is quite acceptable. For averaging times of 1 sec to 100 sec, it exceeds that of the Hewlett-Packard 5061A cesium beam frequency standard, and is comparable to that of commercial rubidiums (see Table 1 for data for $\tau = 100$ sec). Nevertheless, it appears possible to improve the short-term stability further, perhaps by a factor of two or more, if additional effort is expended in this area.

Long-Term Stability (τ = 24 hours)

Measurements of the long-term stability of the pulsed pumping apparatus have been greatly hampered by frequency drifts caused by changes in ambient temperature. There are two basic difficulties. The first is that, at the present time, the apparatus is more sensitive to temperature changes than the commercial unit. This problem is considered further, below. The second problem is that in the room where the apparatus was temporarily set up, there is a 24 hour temperature change of about 7 ^{o}C. At the time of this writing, the apparatus has been moved to a more benign location (where the temperature variation is only 1 to 2 ^{o}C) and measurements are in progress there using the house frequency standard as a reference.

In spite of the difficulties encountered with temperature-induced frequency changes, it has still been possible to obtain some preliminary results on long-term stability and drift. The method used is to take phase comparison data over a period of a couple of days. The data show significant frequency fluctuations that are due to temperature, but these variations are quasi periodic with a period of 24 hours, and are correlated with the 24 hour ambient temperature cycle. If the temperature cycle were exactly periodic and if the apparatus were in a true steady-state condition in response to ambient temperature changes, then any changes in the average frequency from one 24 hour period to the next would be due to long-term frequency instability and drift. If the above conditions are not satisfied, then additional frequency changes due to temperature effects would be superimposed on the long-term stability and drift.

Phase comparison data were taken over a weekend,[22] from 6:30 pm on Friday until 8:00 am on Monday. The maximum frequency (τ = 20 min) variation due to temperature changes during this period was approximately 4×10^{-11}. The phase comparison data were analyzed at 24 hour intervals at times of 6 am and 11 pm. (These times of day were chosen because the frequency then was changing slowly due to temperature.) Table 2 summarizes the results obtained for the average frequencies over these 24 hour periods. It now remains to consider the effect on these results of deviations from the ideal temperature cycle assumed above.

Measurements have been made of the weekend temperature variation in the

room where the stability data were taken. These measurements showed a $-1^{o}C$ temperature change from 11 pm Friday to 11 pm Saturday. All 24 hour changes occuring from Saturday onward were also negative, with magnitude $\leq 0.5\ ^{o}C$. Since the overall temperature coefficient of the apparatus during the stability run[23] was about $5 \times 10^{-12}/^{o}C$, we can therefore conclude that the effect of the deviation from a perfect 24 hour temperature cycle is to introduce a small negative frequency drift of $< 5 \times 10^{-12}$ which is greatest early in the run. Thus, the frequency changes due to temperature effects are expected to be approximately the same sign and magnitude as the changes in average frequency that are recorded in Table 2. It is therefore concluded that changes in the average frequency (τ = 24 hours) over successive 24 hour periods are of order parts in 10^{12} Since the reference used (essentially an FRK-H) cannot be verified (by measurements traceable to NBS) to be stable to better than about 6×10^{-12} for τ = 24 hours, we have to conclude, on the basis of these data, that the long-term stability and drift (τ = 24 hours) for the pulsed optical pumping apparatus are no worse than this. In fact, the results obtained here do not exclude the possibility that the stability of the pulsed device is better than this, and even better than that of the commercial frequency standard. Please see NOTE ADDED IN PROOF, p.68.

TABLE 2. LONG-TERM FREQUENCY STABILITY OVER 24 HOUR PERIODS

Twenty-four hour period	Average frequency (τ = 24 hours)	Change in average frequency
11 pm Fri. to 11 pm Sat.	-1.7×10^{-11}	-5×10^{-12}
11 pm Sat. to 11 pm Sun.	-2.2×10^{-11}	
6 am Sat. to 6 am Sun.	-2.1×10^{-11}	-2×10^{-12}
6 am Sun. to 6 am Mon.	-2.3×10^{-11}	

Additional long-term stability measurements need to be made to characterize adequately the stability over periods of 24 hours and longer. The sensitivity of the output frequency to changes in ambient temperature is an impediment to such measurements, and some effort should be devoted to reducing this sensitivity. Possible ways of doing this are discussed in the next section.

Measurements of long-term stability to better than a few parts in 10^{12} will require that a cesium beam be used as the reference: our present in-house frequency standard is a three-member ensemble. The first two members are especially selected and modified Efratom FRK-H rubidium frequency standards. The third member is the channel 7 (Los Angeles) ABC TV color subcarrier which is locked to a cesium standard at the network originating studio. Over a 24 hour period, the measurement uncertainty for the channel 7 color subcarrier frequency^{24} is 6×10^{-12}. For the ensemble as a whole, the long-term stability is $\lesssim 4 \times 10^{-12}$ for 24 hours (8.6×10^{4} sec), and $\lesssim 2 \times 10^{-12}$ for one week (6.0×10^{5} sec).

Temperature Sensitivity of Output Frequency

There are at least three different ways to reduce the sensitivity of the output frequency to changes in ambient temperature: (1) reduce the temperature sensitivity of the electronics; (2) reduce the resonance cell temperature coefficient; (3) use electronic temperature compensation that senses temperature changes and makes a correction to the output frequency.

The temperature sensitivity of the electronic circuitry has been investigated by cooling circuits and components with spray cooler (i.e., cooling with freon from a pressurized can) while the apparatus is operating as a frequency standard, and observing any associated change in the output frequency. While a comprehensive study has not been carried out using this method, it is still possible to draw certain conclusions. The 5 MHz buffer amplifier and rf switch, and the pulsing electronics are relatively insensitive to temperature changes (they were designed to accomplish this end). On the other hand, the PIN diode phase modulator is sensitive to temperature, especially the five PIN diodes in this circuit. Steps should there-

fore be taken to either redesign this circuit for reduced temperature sensitivity, or to place it in a temperature-controlled oven (a possible experimental expediency). In addition, a systematic spray cooling study of all other circuitry should be undertaken, and corrective action taken where required.

The dependence of the output frequency on the temperature of the Rb resonance cell has been measured over a 16 ^{o}C temperature range.[25] The temperature coefficient is approximately +6.5 x $10^{-10}/^{o}$C. This is about 50% greater than for our commercial unit. This temperature coefficient could be reduced by up to 10 times by using a different combination of buffer gases in the Rb resonance cell.

Electronic temperature compensation (a patented Efratom invention) is used in the Model FRK. Instead of using a separate temperature sensor, the current that is used to heat the microwave cavity and resonance cell is sensed (this current decreases as ambient temperature increases) and a signal derived from this is used to correct the output frequency by changing the C-field current. In fact, this very technique was used when making the long-term stability measurements described in the previous section. For those measurements, the overall temperature coefficient of the unit, with electronic temperature compensation, was roughly 5 x $10^{-12}/^{o}$C. There are, however, two limitations to this technique. First, the improvement in temperature coefficient is limited to about a factor of ten in actual practice. Second, the transient response of the output frequency for rapid temperature changes is not much improved because the different thermal time constants associated with different parts of the apparatus remain the same. Clearly, it is more desirable to reduce the uncompensated temperature sensitivity than to try to compensate for it electronically.

In summary, it appears possible to reduce the sensitivity of the output frequency to changes in ambient temperature by using the methods described above (which are relatively straightforward). This should allow an improvement of about an order of magnitude in the overall device temperature coefficient.

FUNDAMENTAL DEVICE IMPROVEMENT

As noted in the introduction, there are two parallel approaches that have been taken in this work. The first is concerned with frequency stability measurements and the empirical improvement of device stability without regard to the physics of device operation; this approach is described in the previous section. The second approach is an attempt to characterize and improve device operation as a frequency standard by gaining a fundamental understanding of device behavior. This latter approach is considered here (see Figure 3).

Areas of Concern

There are two main areas of concern that have important implications for operation of the pulsed pumping apparatus as a frequency standard. They are the existence of possible residual light shifts, and the dependence of the output frequency on the pulse parameters (and other experimental variables as well). These areas of concern are discussed in the next two sections.

Sensitivity to Pulse Parameters

Figures 10 to 12 show how the output frequency of the pulsed pumping apparatus depends on various pulse parameters. In all three figures, the relevant curve (labeled $\Delta f/f$) is for closed-loop operation as a frequency standard. Since the absolute frequency is not of interest here, only relative frequency differences are presented. As an example, Figure 10 shows that if the light pulse duration is increased from 1.0 msec to 2.5 msec, the output frequency increases fractionally by 3.0×10^{-10}. Experimental conditions for the three $\Delta f/f$ curves are given in Table 3. The Rb lamp and cell temperatures were the same in all three cases.

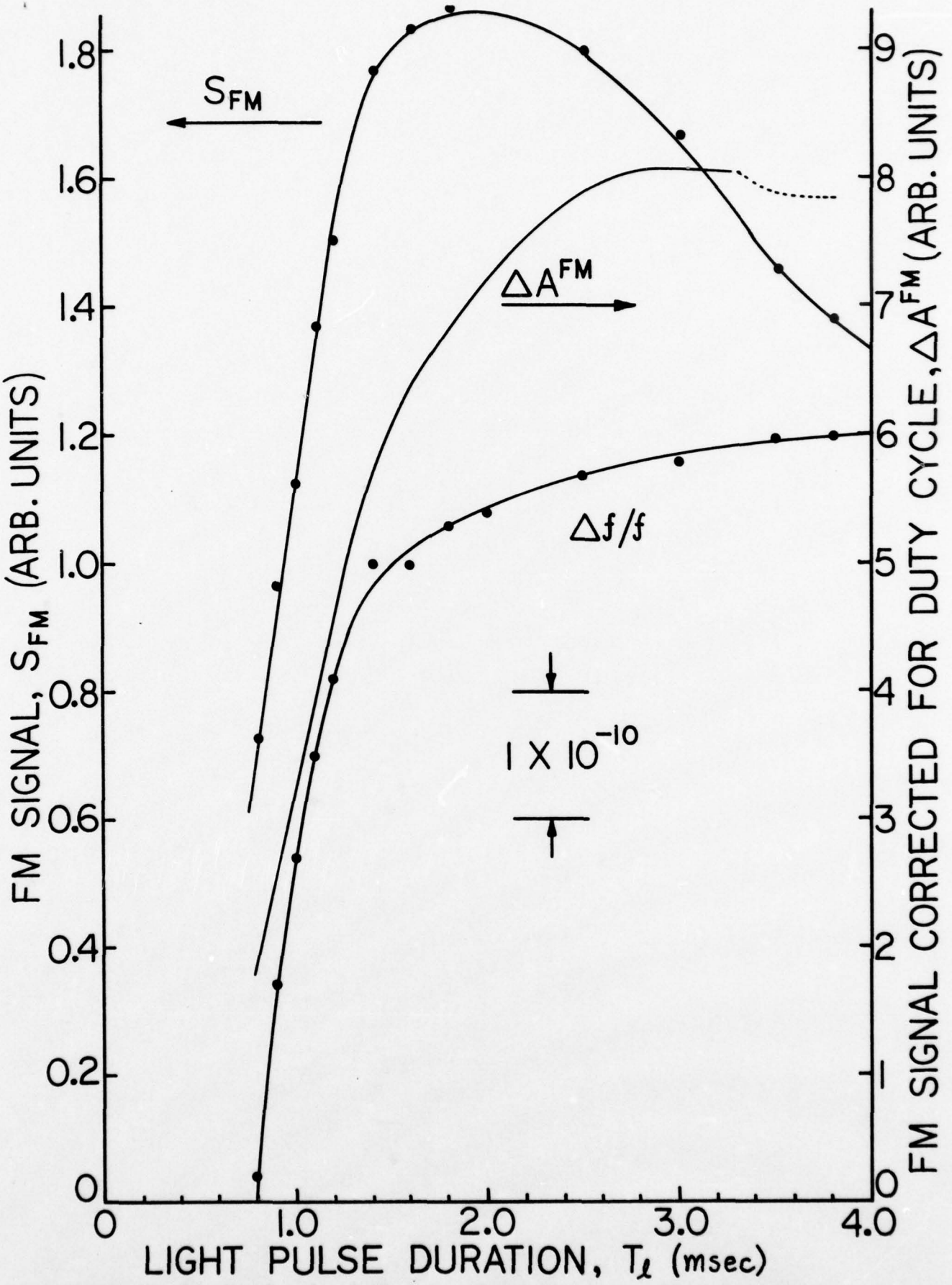

Figure 10. FM signal and relative fractional frequency offset as a function of light pulse duration. See Table 3 for experimental conditions.

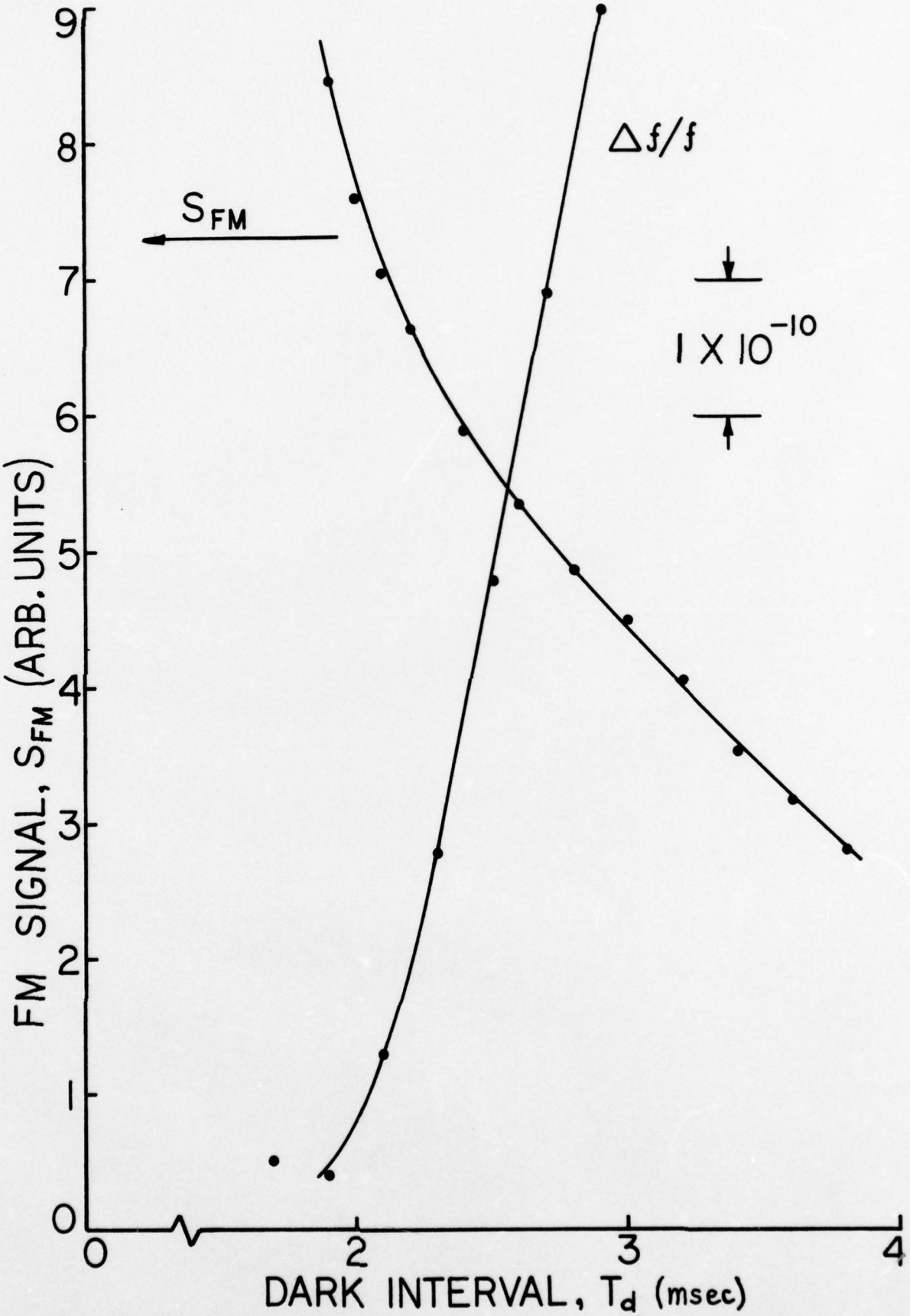

Figure 11. FM signal and relative fractional frequency offset as a function of dark interval. See Table 3 for experimental conditions.

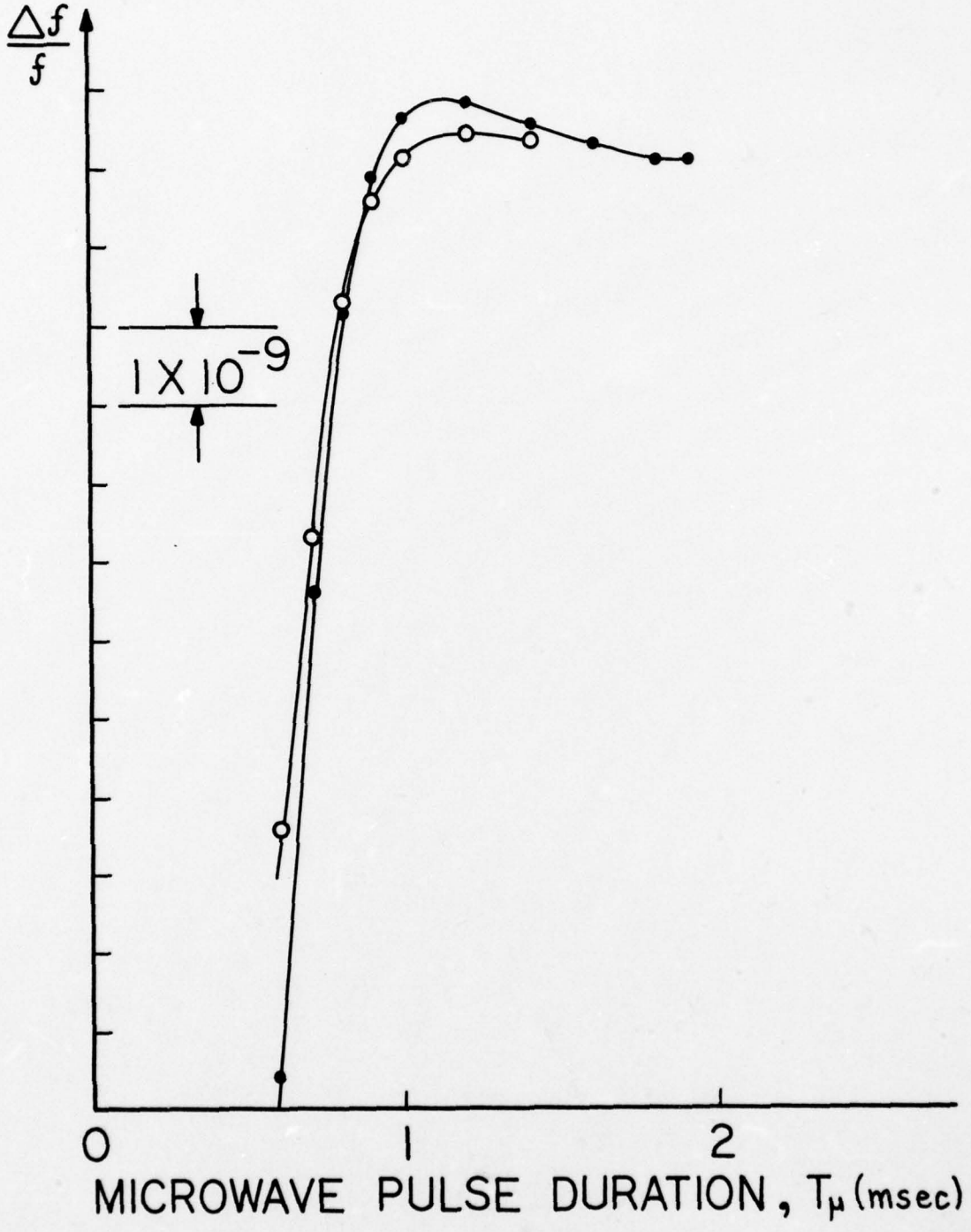

Figure 12. Relative fractional frequency offset as a function of microwave pulse duration. See Table 3 for experimental conditions.

TABLE 3. EXPERIMENTAL CONDITIONS FOR FIGURES 10 to 17

Figure number	Curve	Experimental conditions						
		T_ℓ (msec)	T_s (msec)	T_μ (msec)	T_d (msec)	T_L (^oC)	T_C (^oC)	Lamp no.[a]
10	$\Delta f/f$, S_{FM}, ΔA^{FM}	- -	0.14	1.55	1.9	130	66	110
11	$\Delta f/f$	1.1	0.14	1.55	- -	130	66	110
	S_{FM}	1.8	0.14	1.55	- -	130	66	110
12	●	2.0	0.14	- -	2.1	130	66	110
	O	2.0	0.14	- -	1.6	130	66	110
13		- -	0.14	1.55	1.7	130	66	110
14	A	1.4	0.06	0.55	0.7	121	75	210
	B	- - - cw operation - - - - - -				121	75	585
	C	1.4	0.06	1.1	1.2	121	75	585
	D ●	1.8	0.14	1.55	1.9	130	66	110
	O	1.1	0.14	1.55	1.9	130	66	110

TABLE 3. (CONTINUED)

Figure number	Curve	Experimental conditions						
		T_ℓ (msec)	T_s (msec)	T_μ (msec)	T_d (msec)	T_L (^oC)	T_C (^oC)	Lamp no.[a]
14	E	1.4	0.06	2.0	2.1	121	75	585
	F	1.4	0.06	2.5	2.6	121	75	210
15	S_{AM}, ΔA^{AM}	- -	0.14	1.55	1.9	130	66	110
16	A,B	2.0	0.14	1.0	- -	130	66	110
17	Solid	2.0	0.14	- -	3.0	130	66	110

[a]Lamp nos. 110 and 585 contain both isotopes of Rb; lamp no. 210 contains only ^{87}Rb.

The $\Delta f/f$ curves in Figures 10 to 12 all exhibit a common behavior. There is a region where the frequency is changing very rapidly with the pulse parameter, and another region where the change in frequency is much more gradual. This type of behavior seems to hold generally, and is not dependent on a particular parameter having a specific value. It is therefore possible to choose the operating conditions so that frequency changes due to changes in pulse parameters are minimized, and this is usually done. This procedure is probably adequate to ensure long-term stabilities of several parts in 10^{12} or better over days and weeks,[26] but if stabilities of parts in 10^{13} and 10^{14} are to be obtained over the same periods of time, and longer, then it will probably be necessary to use a more fundamental approach which seeks to reduce the sensitivity of the output frequency to changes in the pulse parameters, and other instrumental parameters as well (see, for example, the discussion of the "position-shift effect" in the next section).

A question of some importance is, do the $\Delta f/f$ curves result from fundamental physical effects, or are they some spurious artifact of the experimental setup? It is difficult to answer this question completely, but it is possible to eliminate a large class of possible artifacts. We have done this by operating the apparatus open loop (the loop is broken between the integrator and the VCXO in Figure 8) and observing the dc component of the signal from the output of the phase detector. (In effect, we are using the signal processing section of Figure 5.) The VCXO is voltage tuned (as in Figure 5) so that the 6.8 GHz is way off resonance, and pulse parameters are then varied. Under these conditions, any spurious effects should show up as a detectable change in the dc output level of the phase detector. No detectable change is observed. The same result is also obtained when the 6.8 GHz is absent altogether. The absence of any change in the dc level as the pulse parameters are varied, eliminates a large class of spurious apparatus effects (e. g., ground loop and/or rf pickup induced signals in the signal processing electronics that originate in the pulsing circuitry). When this type of experiment is carried out with the 6.8 GHz tuned to the peak of the Rb resonance, dc level shifts are observed, but in this case it is not possible to distinguish fundamental effects from spurious ones. To summarize, we have carried out tests to detect spurious effects, such as ground loops and rf pickup, and have detected none. Therefore, in so far

as we can tell, the variation of the output frequency as a function of the pulse parameters is a real effect, and is not just an electronic artifact of the apparatus.

Position-Shift Effect

The so-called "position-shift effect" has been studied[7] by Risley and Busca. This effect is due to inhomogeneous broadening in the physics package, combined with nonuniform excitation (optical pumping) and interrogation of the rubidium atoms as discussed below.

There are two mechanisms that can cause inhomogeneous broadening of the rubidium resonance signal from the physics package. The first is inhomgeneity of the static magnetic field. Since the static field varies over the volume of the Rb resonance cell, ^{87}Rb atoms in different parts of the cell will have slightly different resonant frequencies (Zeeman effect). Another effect which produces a similar end result is the light-shift effect. Due to the light-filtering action of the Rb atoms in the resonance cell, the intensity and spectral distribution of the pumping light varies throughout the resonance cell. In a cw device this gives rise to a light shift that varies throughout the resonance cell. That is, ^{87}Rb atoms at different locations in the cell will have different resonant frequencies due to the light-shift alone. In summary, there is a nonuniform distribution of ^{87}Rb atom resonant frequencies throughout the resonance cell that is caused by two effects. The most important in our unit is due to the inhomogeneity of the static magnetic field. The other, which should be absent (or else very small) in a pulsed pumping apparatus, is due to the light-shift effect.

Inhomogeneity of the above type is not sufficient, by itself, to produce frequency <u>shifts</u>. However, in combination with inhomogeneity in the processes of ^{87}Rb atom excitation and interrogation, frequency shifts can and will occur.[7] This can easily be seen as follows. As discussed above, ^{87}Rb atoms in different regions of the resonance cell have different resonant frequencies. Also, because the optical pumping (excitation to the F = 2 hyperfine level of the ground electronic state) and microwave inter-

rogation is nonuniform over the cell, the relative contributions of various portions of the resonance cell is not uniform over the cell. The observed atomic line shape is therefore a weighted superposition of individual ^{87}Rb line shapes that are slightly shifted in frequency relative to each other. The center frequency and shape of the observed (composite) ^{87}Rb line therefore depends on the details of all these inhomogeneities. If any of these inhomogeneities is subject to change in any way, then there will be a corresponding change in the shape and the frequency at the peak of the observed (composite) ^{87}Rb resonance line. This will, generally speaking, result in a frequency shift of the device when operated as a frequency standard. Even if the peak frequency of the observed resonance line is not shifted, changes in its shape that produce line asymmetry can still cause output frequency shifts. This can happen because the servo system locks the VCXO to the center of gravity of the observed ^{87}Rb resonance line[27] so that the shape is therefore important also.

For our apparatus, the line width (FWHM) is typically about 550 Hz, or about 8×10^{-8} of the rubidium resonance frequency, whereas the spread of ^{87}Rb resonant frequencies throughout the resonance cell is of order, parts in 10^9. These effects therefore constitute a small perturbation on the observed line shape, but they are quite large compared to the precision with which the frequency of the device is to be stabilized ($\sim 1 \times 10^{-12}$ and better).

An example of the type of frequency shift that can occur due to the position-shift effect is that due to microwave power. When the microwave power applied to the microwave cavity changes, then some regions of the resonance cell will be interrogated more strongly, and other regions more weakly. If the regions that are interrogated more strongly have different resonance frequencies than those that are interrogated more weakly, a frequency shift will result.

Risley and Busca[7] have presented evidence which shows that the position-shift effect may be a limiting factor in the long-term stability of

cw, passive Rb frequency standards. In a pulsed optical pumping device, it should be possible to eliminate, or reduce to a negligible value, frequency shifts that are due to the position-shift effect. This can be done by making the static magnetic field more uniform. In the FRK physics package that we are using in the pulsed pumping apparatus, this field is quite nonuniform and a considerable improvement should be easy to obtain. In principle, if the static magnetic field in a pulsed pumping apparatus is completely homogeneous, the position-shift effect should be entirely eliminated. This is not true for a cw apparatus because there is still inhomogeneous broadening due to light shifts. This, therefore is a definite advantage of the pulsed pumping method.

Residual Light Shift

A question of great interest from a practical point of view (and otherwise) is, is there any light shift when pulsed optical pumping is used? For the apparatus that we have constructed, there is a small residual light shift. On the other hand, there is evidence which strongly indicates that this is not a true light-shift effect, but arises instead from a different physical effect. For this reason we will refer to this phenomenon as the "pseudo light-shift effect" (see Figure 3). This residual light shift is discussed below.

An experiment was conducted using two different rubidium lamps, #210 and #110. Lamp #210 contains pure ^{87}Rb, while lamp #110 contains both rubidium isotopes. The spectral distributions of the light from these two lamps are expected to differ greatly and therefore to produce significantly different light shifts in a gas cell rubidium device operating in the cw mode. For operation in the pulsed mode (with no light-microwave overlap), the light shifts are expected to be either absent, or else to be very much smaller in magnitude than the light shifts for cw operation (but of the same sign in each case).[15]

The experiment consisted of first placing lamp #210 in the apparatus. For operation in the cw mode, the fractional frequency of the apparatus,

relative to a fixed reference, was -2.6×10^{-9}. Lamp #210 was then removed and replaced by lamp #110. With the apparatus still operating cw, the fractional frequency, relative to the same fixed reference, was $+3.9 \times 10^{-9}$ for lamp #110. The total frequency shift in the cw mode, upon changing lamps, was therefore $+6.5 \times 10^{-9}$. When the apparatus was operated in the pulsed mode, under the same conditions with the same fixed reference, the fractional frequency offsets were -2×10^{-10} for lamp #210, and -4×10^{-10} for lamp #110. The total frequency shift in the pulsed mode, upon changing lamps, was therefore -2×10^{-10}. Similar experiments with the lamp pulsed and the microwave operated cw (with approximately 50 % light-microwave overlap) gave frequency offsets and shifts that lay ~ halfway between the values for the fully pulsed and the fully cw modes.

The results of this experiment are consistent with the hypothesis that the frequency shift of $+6.5 \times 10^{-9}$ in the cw mode is due mostly to a change in the light shift when lamp #210 is replaced by lamp #110. If this is a valid hypothesis, then the shift of -2×10^{-10} in the pulsed mode (under the same conditions), must be interpreted as due to some effect other than a true light shift because of the opposite sign.[15]

A different way to test for light shifts in the cw and pulsed modes is to measure the frequency shift in each mode as a function of light intensity for a given lamp (by inserting light attenuating filters in the light beam). Such measurements have been made in the pulsed mode for two different light pulse durations, but no such measurements have been made in the cw mode for the same experimental conditions (e.g., lamp temperature and cell temperature). The results for the pulsed mode are shown in Figure 13, where it is seen that the fractional frequency shift is a linear function of light intensity. Although two straight lines are shown in the figure, the uncertainties in the plotted points and circles are of the order of the difference between the two lines. We must therefore conclude that the shift is sensibly independent of light-pulse duration.

Additional measurements were made with each lamp in the pulsed pumping mode by inserting a light attenuating filter in the light beam at the

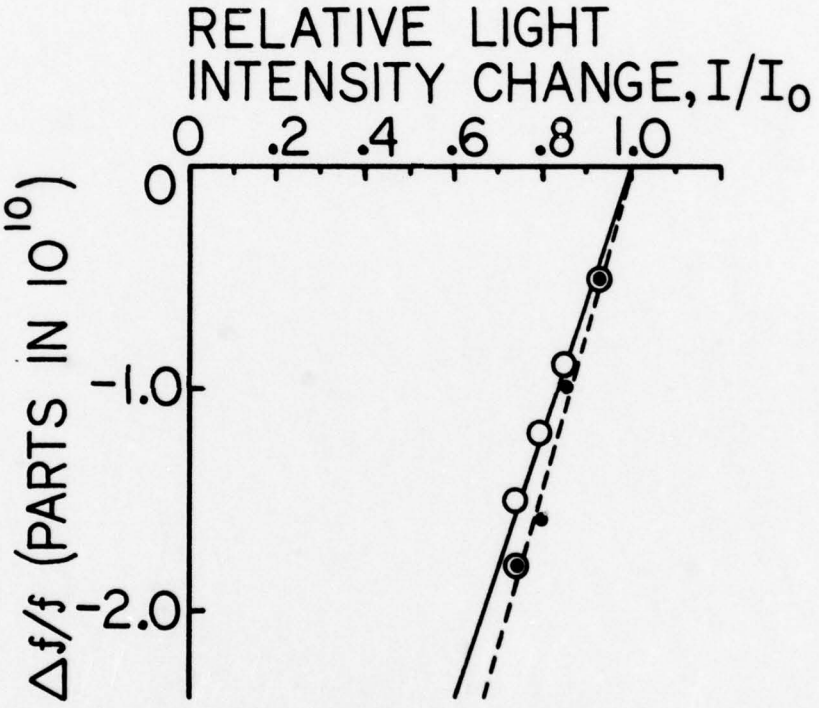

Figure 13. Pseudo light-shift dependence on light intensity. Open circles for T_ℓ = 2.0 ms, dots for T_ℓ = 1.1 ms; other parameters are given in Table 3.

point where it leaves the Rb lamp. It has been previously established that this filter attenuates the Rb D_1 and D_2 lines by 22 %. The effect of the filter is to produce a shift in the output frequency of the unit of -1.6×10^{-10}. The same result is obtained for both lamps (#210 and #110), whereas for a true light shift we expect the shift for lamp #210 to be about half that for lamp #110, and of the opposite sign.

As another check on whether this is a true light shift, we can examine how this filter shift varies with the duration of the dark period (T_d). The theory (with supporting experimental data) developed by Bazarov and coworkers[15] predicts that a true residual light shift decreases in magnitude as T_d is increased. Therefore, we measured the filter shift for T_d = 1.8 msec and T_d = 2.8 msec (other parameters were T_ℓ = 1.1 msec, T_s = 0.14 msec, and T_μ = 1.5 msec). It was found that the filter shift was the same, and equal to -1.6×10^{-10} in both cases. This is contrary to the behavior expected for a true light shift, as noted above.

On the basis of these experiments, it seems highly unlikely that this is a true light shift. At the present time, the origin of this pseudo light shift is not understood. One possibility is that it is due, at least in part, to the position-shift effect: as the light intensity is changed the spatial distribution of excitation (optical pumping) in the resonance cell is also changed, and there is a resulting frequency shift (that is really due to the inhomogeneous broadening by the static magnetic field and has nothing whatsoever to do with a true light shift). One way of checking this hypothesis is to repeat the above measurements with a homogeneous static magnetic field. If the pseudo light-shift effect persists unchanged, then the position-shift effect is not the cause.

In summary, there is a small residual "light shift" when our pulsed optical pumping apparatus is operated as a frequency standard. Various experiments have shown that this shift does not behave like a true light shift. For this reason, we have called it the "pseudo light shift." Although the origin of the pseudo light shift is not presently known, it is possible that it may arise from the position-shift effect. A way of test-

ing this hypothesis has been presented. The dependence of the pseudo light shift on light intensity has been measured (Figure 13), and from these data it is estimated that a 1 % change in light intensity will produce a frequency shift of 6×10^{-12}. From this, it is clear that if the long-term stability of the pulsed pumping apparatus is to be improved beyond its present value of parts in 10^{12}, the pseudo light shift will have to be reduced by at least an order of magnitude. This should be possible if the pseudo light shift is a manifestation of the position-shift effect, but further work will be required to establish this.

Understanding Device Operation

The previous section (Areas of Concern) has shown that there is a definite need to obtain a fundamental understanding of device operation. Reference to Figure 3 shows that some progress along this line has already been made. This is discussed below.

Theoretical Model of Device Operation

The development of a theoretical model of device operation must proceed in two steps. The first is the prediction of how the observed rubidium resonance signal depends on the parameters of the apparatus, and the second is the prediction of how the output frequency depends on the same parameters.

The theory of Bazarov & coworkers[15] treats both aspects of device operation with emphasis on the latter, but it also neglects an important aspect of device operation that is important for our apparatus, namely, inhomogeneous broadening (such as occurs in the position-shift effect). For this reason, we have chosen to develop our own theoretical treatment, as described below. So far, we have not attempted to formulate a theory of the line shape, but our theory could be extended to include this.

Starting with the basic quantum mechanical equations that describe the optical pumping process, we have developed a theoretical model that predicts how the observed signal depends on various apparatus parameters other than microwave frequency, especially the pulse parameters. This theory is briefly outlined in Appendix A. In the next section (AM measurements), the results of an experimental investigation of device properties are presented, and compared with the predictions of this theory. Good agreement between theory and experiment is obtained.

AM Measurements

The AM measurements fall into two categories, as can be seen in Figure 3. Each category is discussed separately below.

Line Shapes

Observed ^{87}Rb resonance (AM) line shapes are shown in Figure 14 for a variety of experimental conditions (as itemized in Table 3). The lamp and cell temperatures are identical for all curves except curve D. For this reason we will discuss curve D last. All curves, except curves A and F, were obtained using lamps that contained both isotopes of Rb. Curves A and F were taken using a lamp containing only ^{87}Rb. The type of lamp used is not expected to have much effect on the line shape on the scale shown in Figure 14.

Curve B shows the line shape for cw operation. In this case the line width[28] is approximately 1100 Hz. However, when the apparatus is operated in the pulsed mode it is possible to obtain line widths as small as 360 Hz (curve F). This shows that under cw conditions light relaxation makes a significant contribution to the resonance line width. This also demonstrates that in the pulsed mode the microwave radiation really does interrogate the atoms when they are in the dark. From the uncertainty principle, it is expected that the line width in the pulsed mode should vary as $1/T_\mu$, where T_μ is the duration of the exciting microwave radiation. For line widths larger than 360 Hz this is the case, and the data show that the line width $\simeq 0.9/T_\mu$. In this regard, it is interesting to note that when T_μ becomes very small, the line width becomes quite large. This is demonstrated

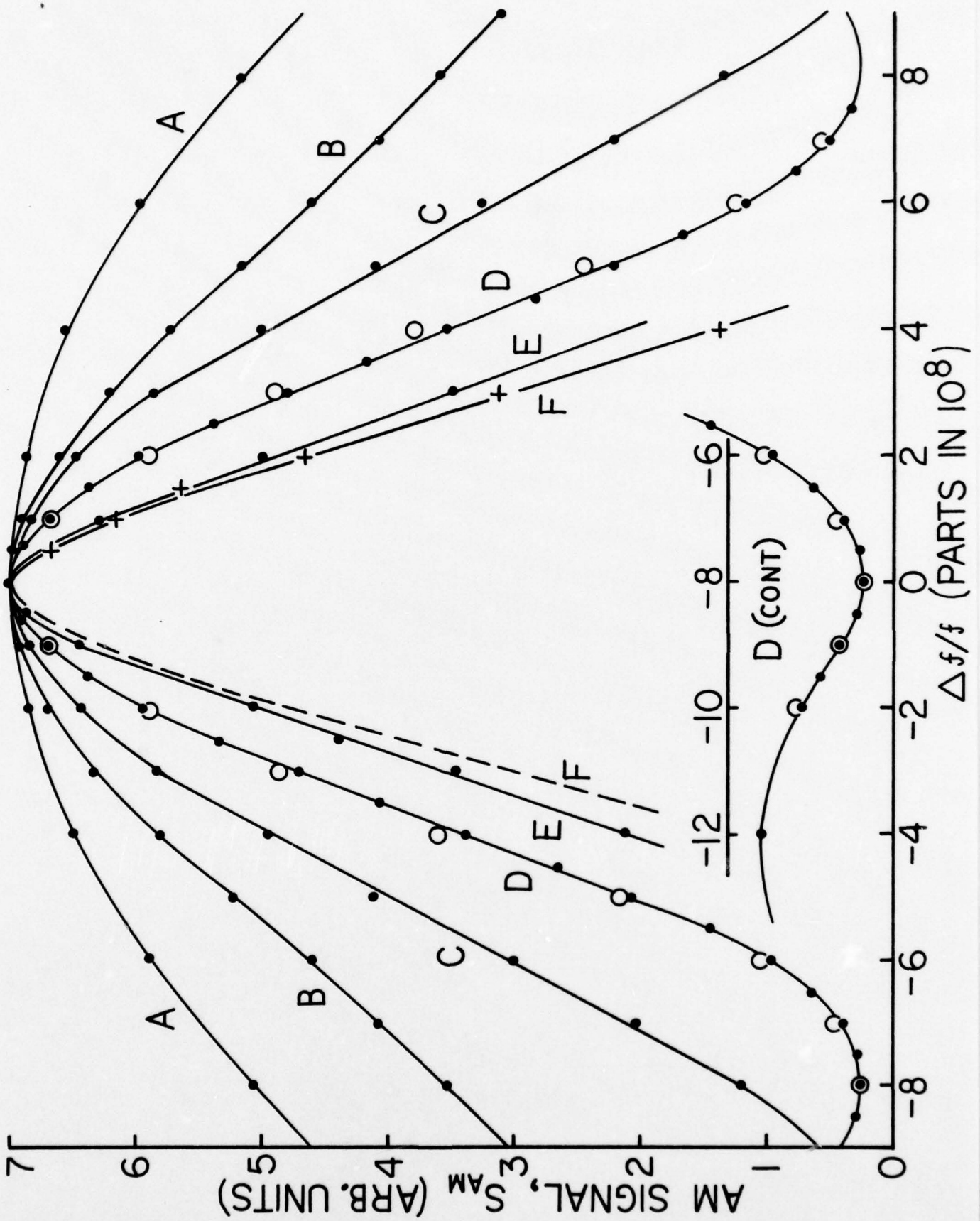

Figure 14. Observed Rb resonance AM line shapes. All curves are normalized to the same value at $\Delta f/f = 0$. Experimental conditions are given in Table 3.

by curve A where the line width for pulsed operation with T_μ = 0.55 msec is about 1700 Hz, which is greater than the cw line width (curve B).

The lower limit on the line width in the pulsed mode is set by inhomogeneity broadening of the static magnetic field, and various relaxation processes. It is estimated that the magnetic field inhomogeneity contributes less than 50 Hz. The contribution due to relaxation is larger than this, and can be estimated from measurements (see the next section) of the relaxation time for the decay of the F=2, F=1 population difference (T_1 in NMR jargon). For a cell temperature of 75 ^{o}C, T_1 = 1.2 msec. Since we do not, at present, have a theory of the line shape, it is not clear whether T_1 or T_2 (relaxation time for decay of the oscillating magnetization) or some combination of the two, is appropriate to use to compute the relaxation contribution to the line width. However, the differences are expected to be small because usually $T_2 \approx T_1$. If we use the experimental value of T_1, the contribution due to relaxation is 260 Hz. To this must be added (directly) the contribution due to inhomogeniety broadening. This gives a final estimate for the total line width of approximately 300 Hz which is in good agreement with the experimental observations (experimental lower limit <360 Hz).

We now discuss curve D. For it, two sets of data were taken, differing only in the values of T_ℓ. The dots are for T_ℓ = 1.8 msec, and the open circles for T_ℓ = 1.1 msec. It is not known if the slight difference observed between these two sets of points is significant. The wing of the line for curve D is also shown separately in Figure 14. The subsidiary maximum is a real effect and has been observed in other line shapes (not shown in Figure 14) when the apparatus is operated in the pulsed mode. This effect is not present when the apparatus is operated in the cw mode. Subsidiary maxima also occur in molecular beam experiments when the beam is monochromatic in velocity.[13,29] In both cases the basic effect is due to the microwave (or radiofrequency) radiation being applied as a pulse.[30]

It might be thought that it would be advantageous to operate the pulsed pumping apparatus using the narrowest possible line width. This is not necessarily the case, however, because the signal strength decreases approximately exponentially with T_μ, whereas the line width decreases only as $1/T_\mu$.

AM Signal as a Function of Pulse Parameters

The AM signal has been studied as a function of the pulse parameters T_ℓ, T_d and T_μ. The variation as a function of light pulse duration is shown in Figure 15. The dots are the experimental data points, and the curve labeled S_{AM} passes through these points. The curve labeled ΔA^{AM} is obtained (except for the overall normalization which is arbitrary) by multiplying the function $S_{AM}(T_\ell)$ by $(T_\ell + T_d)$. According to Eq. (A24), this gives the AM signal corrected for duty cycle, ΔA^{AM}.

The behavior of ΔA^{AM} in Figure 15 is as expected on the basis of the theory developed in Appendix A. Starting with a narrow light pulse the AM signal ΔA^{AM} (corrected for duty cycle effect) increases rapidly at first with light pulse duration, and subsequently approaches saturation. Physically, this can be understood as follows. If the lamp is suddenly turned on (the microwave is assumed to be off for the moment), ^{87}Rb atoms will be pumped out of the F=1 hyperfine level and into the F=2 level. This causes the population of the F=1 level to decrease exponentially with time, approaching an asymptotic value that depends on the intensity of the light and the relaxation rate. Since the light absorption is proportional to the population of the F=1 level, the light absorption will be greatest at first and will also decrease exponentially with pumping time. This type of behavior is shown schematically in Figure 16 for two cases. In the first case, the light pulse duration is $T_\ell = T$. During one half of the 10 Hz modulation cycle, the microwave radiation is not present between light pulses. In the steady state, this gives the lower curve shown in Figure 16. During the other half of the 10 Hz modulation, the microwave pulses are present between the light pulses. Under steady state conditions, this gives the upper curve of Figure 16. In this case, the AM signal corrected for duty cycle, ΔA^{AM}, is proportional to the shaded area that is between the two curves in the interval $T_\ell = 0$ to $T_\ell = T$. If the light pulse duration is increased from $T_\ell = T$ to $T_\ell = T'$ then this adds the additional shaded area[31] between T and T'. Looking at Figure 16, it is now clear why the AM signal (ΔA^{AM} in Figure 15) increases rapidly at first and then approaches saturation as T_ℓ is increased.

The behavior of the AM signal as a function of the dark time T_d has also been investigated experimentally. All experimental parameters except

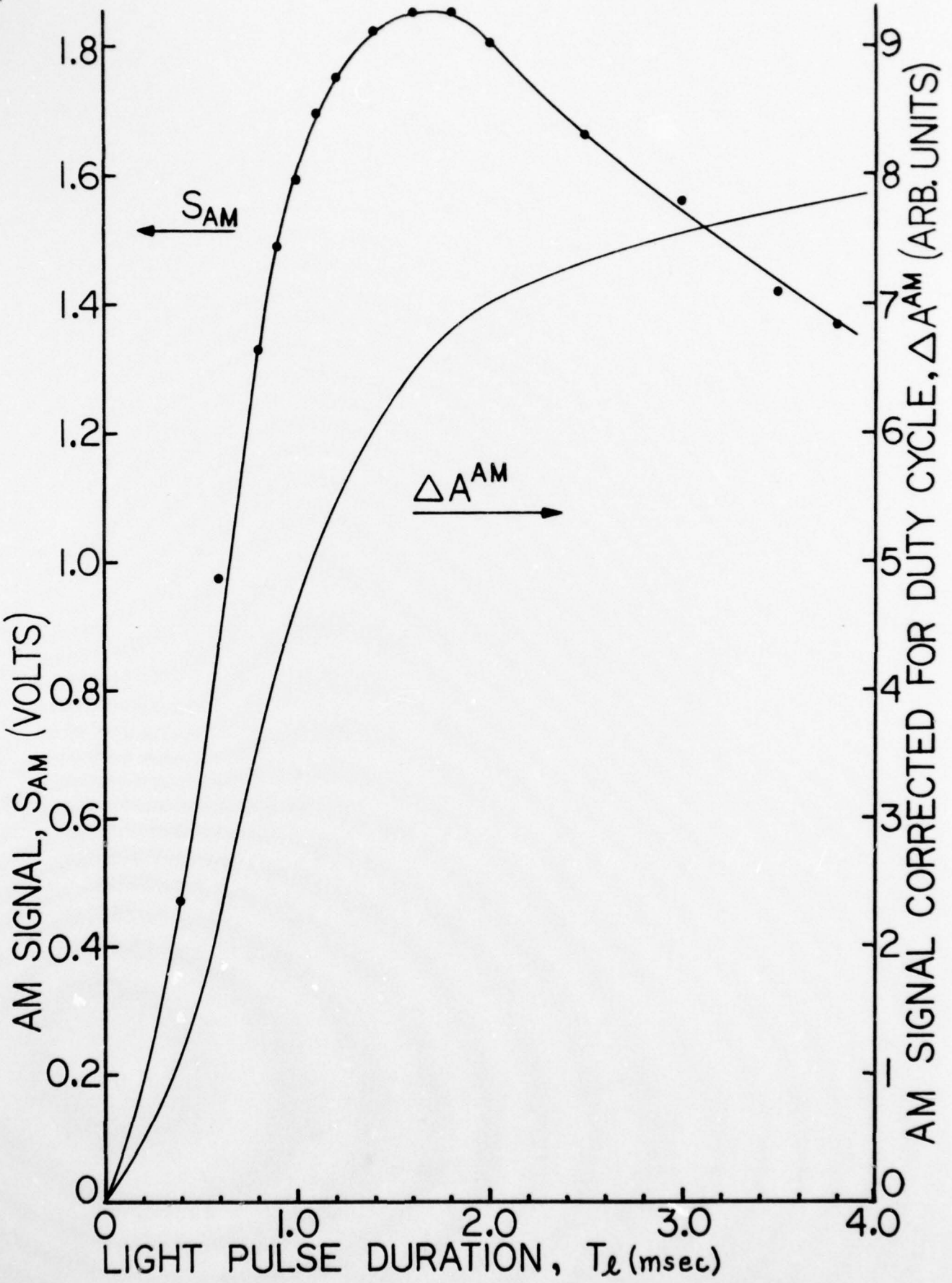

Figure 15. Measured AM signal as a function of light pulse duration. See Table 3 for experimental conditions.

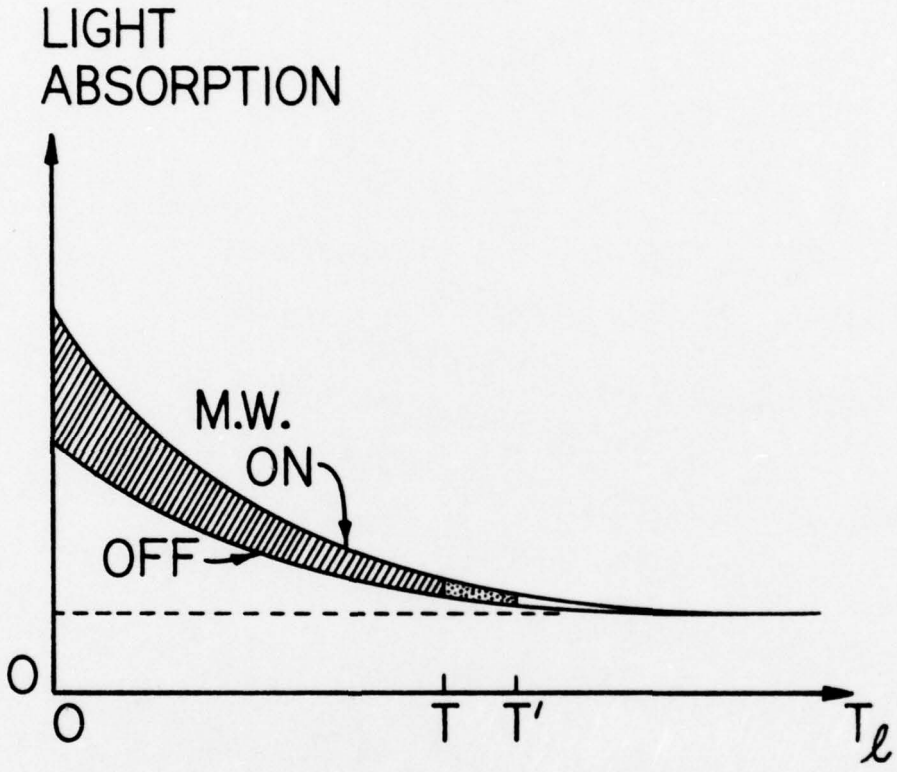

Figure 16. Schematic diagram showing light absorption as a function of pumping time (light pulse duration). The AM signal corrected for duty cycle, ΔA^{AM}, is proportional to the shaded area between the two curves.

T_d are held fixed. Also, T_ℓ = 2.0 msec which ensures that we are operating in the saturation region for ΔA^{AM} (see Figure 15), and T_d is varied in such a way that there is no light - microwave overlap ($T_d > T_s + T_\mu$). Under these conditions, Eq. (A23) applies. This equation shows that in the light-pulse-duration saturation limit, the AM signal ΔA^{AM} (corrected for duty cycle) is proportional to $e^{-\gamma_1 T_d}$. This allows a determination of the relaxation time $T_1 = 1/\gamma_1$ which is the time constant for the decay of the population difference. Figure 17 shows the experimental results for a change in AM signal of > 10:1. According to Eq. (A23), the curve of Figure 17 should be a single straight line. Instead, the data are fit by two straight lines, A-A and B-B. For A-A, T_1 = 1.67 msec, whereas for B-B, T_1 = 1.82 msec. While this effect may be an experimental artifact, it is also possible that it is real.[32] This is further discussed below.

Table 4 summarizes both measured and calculated values of T_1 for various resonance cell temperatures. The resonance cell temperature stated in the table as 66°C is estimated to be accurate to better than ±0.5 °C at the location of the thermocouple. However, there is a qradient, perhaps as large as 1 °C, across the resonance cell. The remaining two values of temperature in Table 4 were measured very early in this work and have large uncertainties (~ ±2 °C).

The contribution of ^{87}Rb-^{87}Rb spin-exchange relaxation to the total T_1 is given in column three of Table 4. These values were obtained by calculating the total Rb pressure in the resonance cell from the measured resonance cell temperature using the equation, $\log_{10} P(\text{torr}) = -4560/T_c(^oK) + 12.00 - 1.45 \log_{10} T_c(^oK)$. The spin-exchange contribution was then calculated from the experimental result of reference 33, namely, $1/(T_1)_{SE} = 6.75 \times 10^7 \text{ sec}^{-1} \times P(\text{torr})$.

In principle, the total T_1 cannot exceed that due to spin-exchange alone. For our apparatus and operating conditions, it expected that contributions to the total γ_1 due to buffer gas relaxation and wall relaxation will be quite small.[34] That is, our experimental values of T_1 should be very nearly equal to the value of T_1 due to spin-exchange alone. The discrepancies that occur in Table 4 may be attributed to numerous systematic errors that can plague this type of measurement: especially errors in measuring temperature, and the existence of temperature gradients (already discussed above); the fact, previously reported,[34] that T_1 depends on the

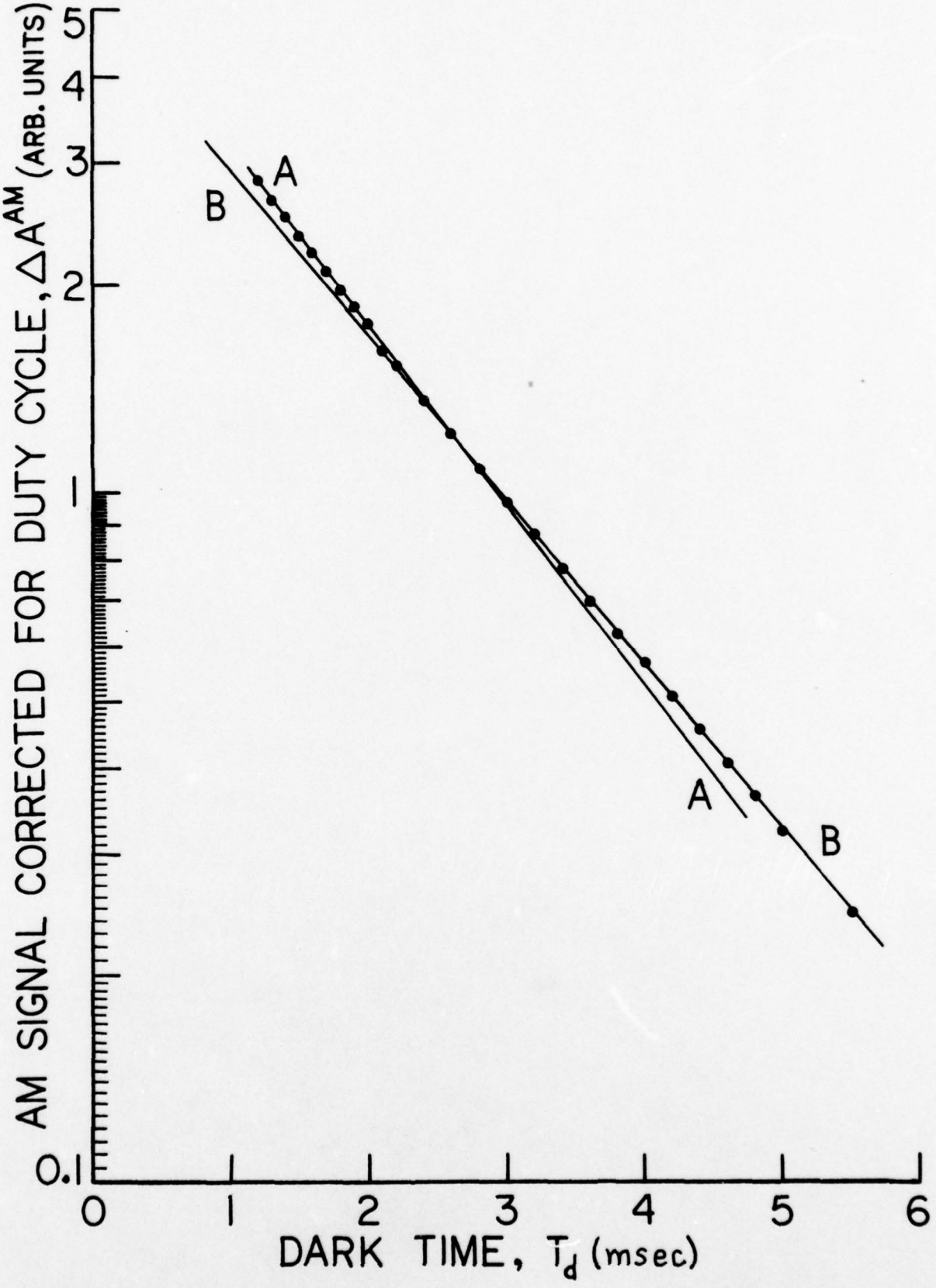

Figure 17. Measured AM signal as a function of dark time. See Table 3 for experimental conditions.

TABLE 4. MEASURED AND CALCULATED RELAXATION TIMES (T_1).

Resonance cell temperature, T_c (^oC)	Relaxation time, T_1 (msec) total experimental[a]	^{87}Rb-^{87}Rb spin-exchange calculated[b]
66	1.67[c,d]	1.95
	1.82[c,e]	
68	1.74[f]	1.64
75	1.19[g]	0.91

[a]Present work

[b]Calculated from the experimental data of reference 33.

[c]Data taken for 11:1 change in ΔA^{AM}, and could not be fit by a single straight line.

[d]From slope of straight line A-A, Figure 17.

[e]From slope of straight line B-B, Figure 17.

[f]Data taken for 3:1 change in ΔA^{AM}, and could be fit by a single straight line.

[g]Data taken for 5:1 change in ΔA^{AM}, and could be fit by a single straight line.

history of the resonance cell and the location of the rubidium within it, in addition to the cell temperature; the same considerations just mentioned, applied to the experimental data and analysis of reference 33.

One other possible source of discrepancy in comparing columns two and three of Table 4 should also be mentioned. The measurements of reference 33 were made using resonance cells filled with ^{87}Rb. Our resonance cell contains both isotopes of Rb, so that spin-exchange relaxation of the ^{87}Rb is due to ^{87}Rb-^{85}Rb collisions as well as to ^{87}Rb-^{87}Rb collisions. Since the nuclear spin can have a significant effect on relaxation due to spin exchange,[32] it is possible that there are two relaxation times, one for ^{87}Rb-^{87}Rb collisions and another for ^{87}Rb-^{85}Rb collisions. If this is the case, then it would not be surprizing to observe two different decay curves. This might be the origin of the two decay curves seen in Figure 17.

The AM signal S_{AM} as a function of microwave pulse duration T_μ is shown in Figure 18 as a solid curve. (In this case, no correction for duty cycle is required because the duty cycle factor $(T_\ell + T_d)^{-1}$ is constant.) An intriguing characteristic of this curve is the presence of two maxima, and because of this it is of interest to compare the experimental result with theoretical predictions. Since the experimental conditions (Table 3) were such that the light pulse duration was in the saturation region, the simplified theory in Appendix A can be used. Three levels of sophistication are possible. We discuss them in order of increasing complexity.

First, we consider the result obtained in the very simple case where the microwave magnetic field, and the optical pumping are uniform throughout the resonance cell. The predicted dependence of AM signal S_{AM} is given by Eq. (A21) multiplied by the factor $1/(T_\ell + T_d)$, as per Eq. (A24). This equation is not plotted in Figure 18 because it is obvious by inspection that it gives a poor fit to the data. It does, however predict successive maxima, but the minima are predicted to be much too deep, and successive peaks are too far apart.

The next degree of sophistication is Eq. (A27), which is obtained by averaging Eq. (A21) over the resonance cell, as explained in Appendix A. Physically, Eq. (A27) holds for a microwave magnetic field that varies as half of a sine wave over the length of the resonance cell, and for con-

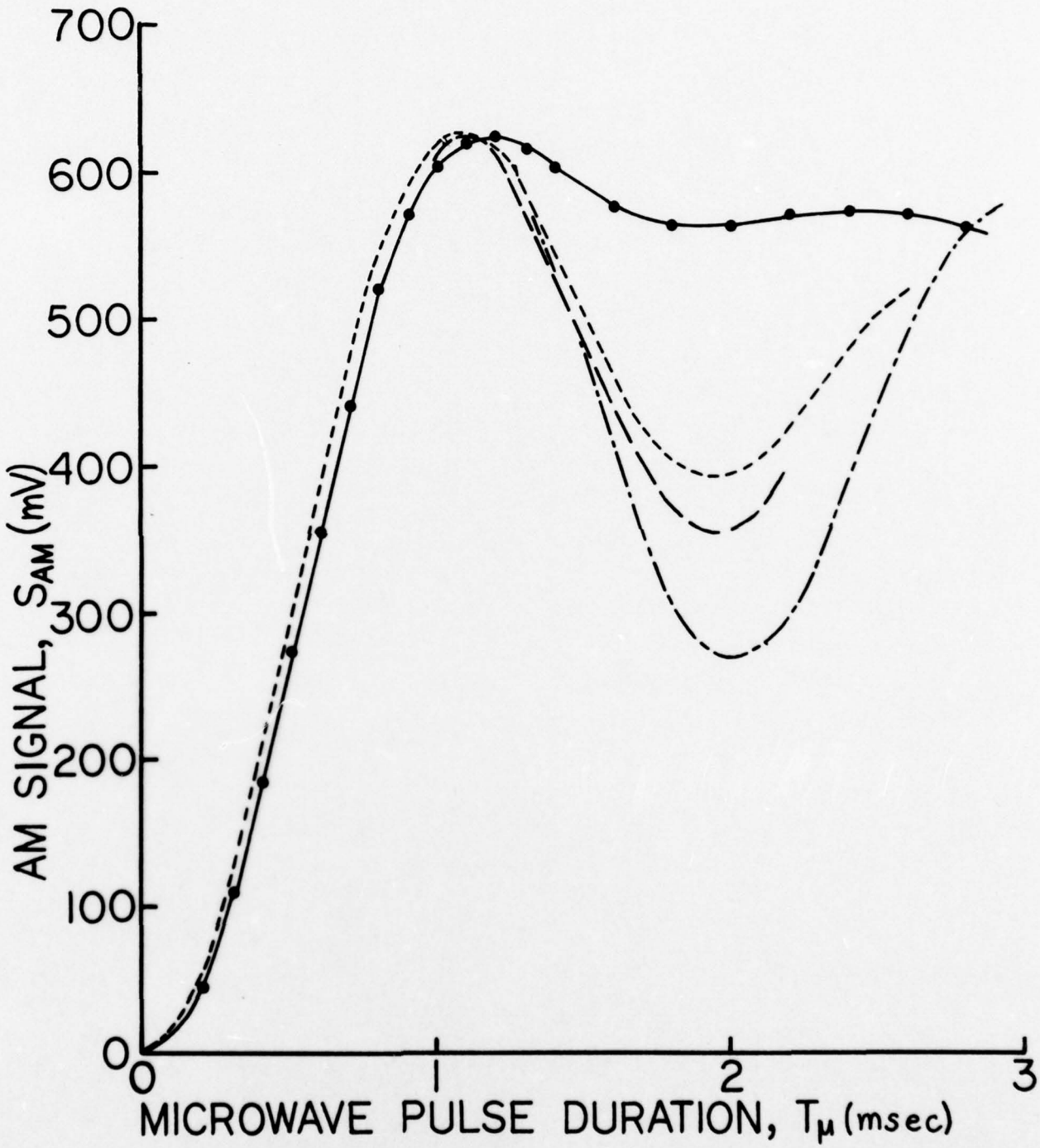

Figure 18. AM signal as a function of microwave pulse duration. Solid curve (and points) are measured; other curves are theoretical. See Table 3 for experimental conditions.

stant optical pumping over the length of the cell. This equation, when normalized and fit to the first peak in Figure 18 gives the dash-dot curve shown there. In plotting this curve, $\Delta\gamma = 210\ \text{sec}^{-1}$ was assumed. This value of $\Delta\gamma$ is the value that results if it is assumed that all relaxation is due to ^{87}Rb-^{87}Rb spin-exchange so that[34] $T_2 = (8/5)\ T_1$, and the experimental value of T_1 from Table 4 is used ($T_1 = 1.8$ msec). The dash-dot curve is an improvement over the prediction of Eq. (A21), but it still suffers from the same basic drawbacks.

The final degree of sophistication that we have considered results from assuming that the optical pumping is much greater at the end of the resonance cell, than at the entrance[7] (see Figure A3), and that the microwave field variation is the same as before. As noted in Appendix A, numerical calculation is required under these assumptions. The result for $\Delta\gamma = 210\ \text{sec}^{-1}$ is shown in Figure 18 as the large-dash curve. For $\Delta\gamma = 0$, the small-dash curve is obtained instead. The best fit is obtained for $\Delta\gamma = 0$. The parameter $\bar{\beta}_0$ is adjusted to give the best fit. For both curves, $\bar{\beta}_0 = 1600\ \text{sec}^{-1}$ was used. This corresponds to a z-component of microwave magnetic field amplitude at the center of the cell of approximately 360 μG.

Figure 18 shows that the theory is over simplified, but it also shows that it contains a great deal of the truth. The deficiencies of the theory probably lie more in the assumptions made when averaging over the resonance cell, than in the basic (quantum mechanical) theory. For example, since the static magnetic field is not uniform in magnitude or direction (as assumed in all cases above), the z-component of the microwave field H_z is not the only component that is effective in inducing the 0-0 hyperfine transition. Also, H_z depends strongly on azimuthal angle as well as on z, but the former was ignored in the theoretical treatment. It is likely that if these effects were taken into account, the sharp dips in the theoretical curves of Figure 18 would be smoothed out.

FM Measurements

The variation of the FM signal S_{FM} was also investigated as a function of the pulse parameters. The procedure used was to open the servo loop between the integrator and the VCXO (see Figure 8); to replace the VCXO by a more stable 10 MHz source; to tune this source slightly off re-

sonance, thereby giving a nonzero FM signal in accordance with Figure 9 (care was taken to remain on the linear portion of the discriminator characteristic of Figure 9); to replace the integrator of Figure 8 by the low pass filter and chart recorder of Figure 5. The variation of S_{FM} was then studied as a function of light pulse duration (T_ℓ) and dark time (T_d). The results, which are shown in Figures 10 and 11, are qualitatively similar to the AM results. In Figure 10, S_{FM} increases rapidly at first, reaches a maximum, and then falls off gradually. ΔA^{FM}, the FM signal corrected for duty cycle, increases rapidly at first and then reaches a saturation condition. This is very similar to the corresponding AM behavior of Figure 15. Quantitatively, differences are observed. For example, the peak of the S_{FM} curve is at T_1 = 2.0 msec, whereas the peak of the S_{AM} curve is at T_1 = 1.7 msec.

Figure 11 shows the FM signal S_{FM} as a function of dark time T_d. If this curve is plotted on semilog paper, the experimental points cannot be precisely fit by one or two straight lines, but an approximate fit can be obtained using a single straight line. For this straight line, T_1 = 1.76 msec. This is very nearly equal to the average of the two values of T_1 obtained from the AM measurements at the same resonance cell temperature of 66°C (see Table 4).

When FM is used, the derivative of the resonance curve is obtained for small modulation index. However, signal/noise considerations require that a large modulation index be used, in which case the FM line shape is not simply related to the Rb resonance curve.[35,36] For this reason, it is difficult to interpret quantitatively the FM measurements.

SUMMARY AND CONCLUSIONS

1. Technical Feasibility

The design philosophy adopted in the present work is that it is not profitable to conduct laboratory experiments using principles and methods that cannot subsequently be applied to the development of a compact, light

weight, low power frequency standard.[37] In keeping with this design philosophy, all experimental work described in this report has been carried out using a very small physics package (consisting of lamp, "integrated cell," microwave cavity, magnetic shield, photodetectors, and lamp electronics) that occupies a total volume of 260 cc (about equal to the volume of an orange.) Using this physics package, it has been demonstrated that the method of pulsed optical pumping is technically feasible in the sense that signal-to-noise ratios can be obtained that are adequate for operating the device as a frequency standard. This is possible because of a dual photocell compensation method that was developed in the course of this investigation.

2. Short-Term Frequency Stability (τ = 1 to 100 sec.)

The short-term frequency stability has been measured for the pulsed optical pumping frequency standard described above. The result is

$$\sigma_y(\tau) = 2 \times 10^{-11}\ \tau^{-\frac{1}{2}}, \qquad 1 \leq \tau \leq 100 \text{ sec.}$$

When the pulsed pumping apparatus is operated cw (no pulsing) the improvement in σ_y is less than a factor of two.

It should be pointed out that the σ_y obtained for pulsed pumping is comparable to that of present-day commercial rubidiums, and exceeds that of commercial cesiums (see Table 1) for the same averaging times. Also, it is possible that this σ_y could be improved, perhaps by a factor of two, with further work.

3. Long-Term Frequency Stability (τ = 24 hours)

Preliminary measurements of long-term stability indicate that the 24 hour average frequency of the pulsed optical pumping frequency standard does not change by more than several parts in 10^{12} from one 24 hour period to the next, and may actually be better than this. At the present time, our verifiable (by measurements traceable to NBS) in-house measurement capability is $\leq 4 \times 10^{-12}$ for τ = 24 hours. Please see NOTE ADDED IN PROOF, p. 68.

4. Temperature Coefficient of Frequency

Over a 10 ^{o}C range of ambient temperature, the temperature coefficient (TC) of frequency of the pulsed optical pumping frequency standard is approximately +5 x $10^{-12}/^{o}$C. This is within a factor of two of the TC of the company's commercial rubidium.[3] For the pulsed device, both the electronics and the Rb resonance cell are temperature sensitive, and it should be possible to make significant improvements in both areas. For example, by using a different combination of buffer gases in the resonance cell, it should be possible to reduce the resonance cell TC by nearly a factor of 10.

5. Light Shift

The light shift was investigated for both cw and pulsed operation by using two different Rb lamps (each of which gives a different light shift for cw operation.) When the pulsed optical pumping apparatus is operated cw, a frequency shift (light shift) of +6.5 x 10^{-9} occurs when the lamp is changed. For pulsed operation, the frequency shift is -2 x 10^{-10} under the same conditions. It is unlikely that this residual frequency shift of -2 x 10^{-10} in the pulsed mode is a light shift because it has the opposite sign, but even if it were, the pulsed mode would still provide more than a factor of 30 reduction.

This frequency shift in the pulsed mode has been investigated and found to be proportional to light intensity, but various experiments that we have carried out show that this shift does not behave like a true light shift. In our opinion, this shift is not a true light shift, and henceforth we therefore refer to it as the "pseudo light-shift effect."

The pseudo light-shift effect is not just of academic interest. It is large enough that a 1% change in light intensity produces a frequency shift of approximately 6 x 10^{-12}. It is therefore of great importance to understand the origin of this effect, and to reduce (or eliminate) it. The likelihood of accomplishing this is considered below (see conclusion 7, "Position Shift Effect".)

6. Dependence of Frequency on Pulse Parameters

It is found that if the values of the pulse parameters of the pulsed pumping frequency standard are changed, the output frequency changes. For each pulse parameter investigated (T_ℓ, T_μ, T_d). it is found that there is a range of values where the frequency changes quite rapidly, and another (separate) range of values where the frequency changes much more slowly. In general, it has been found that it is possible to choose parameter values so that the sensitivity of the output frequency to small changes in parameter values is minimized. In general, this can be done without having to sacrifice signal. This approach appears adequate for stabilities of a few parts in 10^{12} over days and weeks, but if stabilities of parts in 10^{13} and 10^{14} are to be realized over the same periods of time (and longer), then it will be necessary to use a more fundamental approach.

7. Position-Shift Effect

The "position-shift effect" occurs[7] in frequency standards of the type used in this work. It is due to inhomogeneous broadening in the physics package, combined with spatially nonuniform optical pumping and interrogation of the ^{87}Rb atoms. In general, only two sources of inhomogeneous broadening are possible: that due to a nonuniform static magnetic field (C-field nonuniformity) and that due to a true light shift.

Based on the NBS findings,[7] it is virtually certain that the pseudo light-shift effect is due, at least in part, to the position-shift effect. Indeed, if there is no true light shift in the pulsed mode, as we believe to be the case, then the position-shift effect could be completely eliminated by homogenizing the static magnetic field (C-field); this would remove the only remaining source of inhomogeneous broadening. Since the static field in our physics package is very nonuniform, its homogeneity could easily be improved, and the position-shift effect significantly reduced. Therefore it might be possible, by using this simple modification, to greatly reduce the pseudo light-shift effect. This modification should also reduce the sensitivity of the output frequency to changes in microwave power.[7]

8. Theoretical Model of Device Operation

As part of this work, a simple theoretical model of device operation has been developed that provides a simple, conceptual picture of how the signal at resonance depends on device parameters, especially the pulse parameters. The theoretical predictions of this model are found to be in semiquantitative agreement with the experimental results. With further work it should be possible to extend this theory to allow predictions of line shapes as well. The importance of this model is that it provides a conceptual basis for understanding the physics of device operation, which is important for a fundamental approach to device improvement.

9. Relaxation Times

A knowledge of relaxation times is also important for a fundamental understanding of device operation. One of the results of this work has been the development of a new method for the measurement of the relaxation time T_1 (time constant for decay of the population difference.) This method is complementary to previous methods.[33,34]

Measurements of T_1 for our experimental conditions show that the dominant relaxation mechanism is spin-exchange. Our best set of measurements provides evidence for the presence of two distinct relaxation times. While this might be due to a spurious instrumental effect, it could also be due to two differing values of T_1 for our apparatus: one for ^{87}Rb-^{87}Rb spin-exchange relaxation, and the other for ^{87}Rb-^{85}Rb spin-exchange relaxation. If this result is real, it would be of considerable interest because the ^{87}Rb-^{85}Rb spin-exchange relaxation rate has not been previously measured.

10. Line Shapes

The rubidium resonance line shapes for both pulsed and cw operation have been measured. From this, the following conclusions can be drawn. (1) For line widths greater than about 360 Hz, the line width is proportional to $1/T_\mu$ where T_μ is the duration of the microwave pulse. (2) The "intrinsic" line width for pulsed operation in our apparatus is approxi-

mately 300 to 350 Hz and is due almost entirely to spin-exchange relaxation. (3) For cw operation, the line width is approximately 1100 Hz and is due mostly to light relaxation. Therefore, for our experimental conditions, narrower line widths can be obtained when the apparatus is operated in the pulsed mode. (4) The line shapes for pulsed operation show small subsidiary maxima in the wings of the line. This type of line shape has also been observed in molecular beam experiments, and is due to the pulsing of the microwave radiation.

RECOMMENDATIONS

1. Long-Term Stability Measurements

Phase comparison data should be taken for the pulsed optical pumping frequency standard over a period of several weeks, or more. This will allow calculation of $\sigma_y(\tau)$ for $\tau = \geq 24$ hours. Such an effort is currently in progress under controlled environmental conditions using the house frequency standard as a reference. These measurements will most likely be limited by the verifiable (traceable to NBS) stability of the house standard to a precision of $< 4 \times 10^{-12}$ for $\tau = 24$ hours (8.6×10^4 sec), and $< 2 \times 10^{-12}$ for $\tau = 1$ week (6×10^5 sec). If these measurements yield a $\sigma_y(\tau)$ that is limited by the stability of the reference, then it will be necessary to have access to a more stable (for $\tau \geq 24$ hours) reference to establish the true value of $\sigma_y(\tau)$ for the pulsed optical pumping frequency standard. Perhaps ONR could arrange for a cesium beam standard to be made available for such measurements. Other possibilities may also exist.

2. Pseudo Light Shift

The pseudo light-shift effect, as it presently exists, is expected to limit the long-term stability ($\tau < 6 \times 10^5$ sec) to a few parts in 10^{12}. For this reason, it is important that this effect be reduced (or eliminated). More data need to be taken to establish clearly how this effect de-

pends on device parameters, and to determine its physical origin (i.e., is it due solely to the position-shift effect, or are additional physical mechanisms involved?). Also, to the extent that it is due to the position-shift effect, it should be possible to reduce it significantly by improving the C-field homogeneity (which is easy to do). Therefore, this approach should definitely be tried.

3. Position-Shift Effect

It has been established[7] that the position-shift effect is responsible for frequency changes due to changes in light intensity (a form of pseudo light shift) and microwave power. Improvement of C-field homogeneity should therefore be made to see how this affects the pseudo light shift.

At the present time, no investigation of the effect of microwave power on output frequency has been made. This should be examined, at least briefly. If there is a significant dependence, it should be reduced by homogenizing the C-field. Another approach that can be used is to replace the present rf circuit board by one that gives a more amplitude stable output (such a board is presently available to us.)

4. Frequency Shifts due to Changes in Pulse Parameters

This effect will affect the long-term stability at the level of parts in 10^{13}. Therefore, understanding this effect has lower priority than understanding the pseudo light-shift effect. Nevertheless, an understanding of the pulse parameter effect is desirable because it is likely that there are physical mechanisms that are common to both it and the pseudo light-shift effect. Also, it is unreasonable in practice to attempt to separate rigidly these two effects. All of these various effects are surely interrelated, and complete confidence in device operation will require at least a rudimentary understanding of their origin.

5. Effect of Pulsing on Microwave Spectrum

It is well known[38] that the effect of pulsing a sinusoidal wave is to

generate sidebands that are placed symmetrically about the carrier frequency. These side bands are equally spaced, with the spacing between adjacent frequency components being equal to $1/T_\mu$ where T_μ = microwave pulse duration. The amplitude of these components is determined by the pulse repetition rate. The effect of these additional microwave frequencies on device operation should be examined to see, for example, if it is possible to lock the atomic resonance to one of these components rather than to the carrier frequency. The possibility of frequency pulling by sideband asymmetry should be studied in addition. Also, the large frequency shifts that occur as a function of T_μ, when T_μ is small, (see Figure 12) may be related to the amplitude and location of these sidebands in some way. This is an area that demands investigation.

6. Temperature Coefficient of Frequency

At the present time, an integrated (resonance) cell is being fabricated which uses a combination of buffer gases that is designed to reduce the resonance cell temperature coefficient (TC). This should demonstrate the extent to which the resonance cell TC can be compensated using physical mechanisms, and whether this approach will result in reduced signal-to-noise ratios.

Stabilization of the electronics against changes due to variations of ambient temperature is basically an engineering problem, rather than a question of principle. For this reason, stabilization should be carried out only to the extent required for meaningful long-term stability measurements.

7. Theoretical Model of Device Operation

The present model should be extended only to the extent required to aid in accomplishing objectives 2 through 4, above. Emphasis on model development should be placed on the averaging processes that occur in the resonance cell, and on understanding the observed line shapes. For understanding device operation as a frequency standard, the theoretical approach should be extended to include FM operation.

ACKNOWLEDGEMENTS

We would like to thank Werner Weidemann, Engineering Manager of Efratom Systems Corporation, for many helpful discussions, and for kindly making available both equipment and facilities, as needed. We also acknowledge the technical assistance of Jeff Hayner, Henry Holtermann, John Hall and Tom Platt. Thanks are due Judy Yerger for her patience in typing this report, and to Harry Whitmore for the art work.

NOTE ADDED IN PROOF

As this report goes to press, a value of $\sigma_y(\tau) = 4 \times 10^{-12}$ for $\tau = 9 \times 10^4$ sec (24 hours) has been obtained for the long-term frequency stability of the pulsed optical pumping frequency standard (see below.) $\sigma_y(\tau)$ is the square root of the Allan pair variance[19] for four samples of fractional frequency (M = 4), each having an averaging time τ. The statistical uncertainty of σ_y in this case is approximately 50 %.

During the four day period that the data were taken the maximum variation in ambient temperature was 1.6 ^{o}C. The variation in the average ambient temperature during successive 24 hour periods was a few tenths of a degree centigrade at most. Also, the unit had been operating for more than 24 hours when the data taking began. Fractional frequency changes due to temperature effects should therefore amount to $\sim 1 \times 10^{-12}$ or less.

The house standard was used as the frequency reference in these measurements and, as already stated in this report, may be a limiting factor in the value of σ_y that has been obtained above.

It should be noted that the result for σ_y reported here serves to reinforce the conclusions of this report.

REFERENCES

1. NBS Seminar on Frequency Standards and Clocks, Boulder, Colorado, April 6-9, 1976, unpublished notes.
2. Efratom Model FRK Rubidium Frequency Standard, manufactured by Efratom California, Inc., Irvine, Calif.
3. Efratom, Model FRK-H Rubidium Frequency Standard, manufactured by Efratom California, Inc., Irvine, Calif.
4. NBS test results.
5. Rockwell International, Anaheim, Ca., unpublished test results.
6. See for example, M. Arditi and T. R. Carver, Phys. Rev. 124, 800 (1961).
7. A. S. Risley, Final Report on the Microwave-Power and Lamp-Temperature Dependence of the Frequency of a Passive Rb^{87} Frequency Standard, NBS final report to SAMSO, under Air Force contract # SMS 70105, 1978; A. S. Risley and G. Busca, Proceedings 32nd Annual Symposium on Frequency Control, Atlantic City, June 1978.
8. B. S. Mathur, H. Tang, and W. Happer, Phys. Rev. 171, 11 (1968)
9. M. Arditi, U. S. Patent 3,234,483 dated Feb. 8, 1966.
10. M. Arditi and T. Carver, IEEE Trans. Instr. Meas., June - Sept. 1964, p. 146.
11. N. N. Yakobson, "Signals and line shape during the observation of magnetic resonance in alkali metal vapors by pulse pumping," Opt. Spectrosc. 35, 233-237 (1973). Theory only.
12. E. N. Bazarov and V. I. Grigor'yev, "A Study of the Frequency Shift of $S_{1/2}$, F = 2, $m_F = 0 \leftrightarrow S_{1/2}$, F = 1, $m_F = 0$ Transition of Rb^{87} Atoms for Pulsed Optical Pumping," Radio Engineering and Elect. Phys. 14, 912-918 (1969).
13. N. F. Ramsey, Molecular Beams (Oxford, 1956), p.p. 124-134.
14. E. I. Alekseyev, E. N. Bazarov and G. I. Telegrin "Optical Indication of the Ramsey Structure of the Line of the 0 - 0 Transition of Rb^{87} Atoms," Radio Eng. and Elect. Phys. 19, 88-91 (1974).

15. E. I. Alekseyev, E. N. Bazarov and G. I. Telegin, "Light Shifts in a Quantum Frequency Standard with Pulsed Optical Pumping and Optical Indication of the Ramsey Structure of the 0 - 0 Transition Line of Rb^{87} Atoms", Radio Eng. and Elect. Phys. 20, 73-80 (1975).

16. E. I. Alekseyev, E. N. Bazarov and G. I. Telegin, "The Change in the Ramsey Structure of the 0 - 0 Transition Line of Rb^{87} Atoms with an Increase in the Number of Microwave Pulses in the Intervals between the Optical Pumping Pulses, "Radio Eng. and Elect. Phys. 20, 145-147 (1975).

17. J. Viennet, C. Audoin and M Desaintfuscien, Proceedings 25th Annual Symposium on Frequency Control, Fort Momouth, N. J., 1971, p. 337.

18. E. Jechart, "Miniaturized Atomic Frequency Standard," Measurements and Data Magazine, March-April, 1976, p. p. 96-99.

19. D. W. Allan, J. H. Shoaf and D. Halford, "Statistics of Time and Frequency Data Analysis, "Chapter 8 in Time and Frequency: Theory and Fundamentals (NBS Monograph 140, Byron E. Blair, editor, 1974).

20. T. English, unpublished notes.

21. J. H. Shirley, J. Appl. Phys. 34, 789 (1963). See also, NBS Seminar on Frequency Standards and Clocks, Boulder, Colorado, April 6-9, 1976, unpublished notes.

22. Unfortunately, the number of 24 hour periods in a weekend is not sufficient to allow calculation of the Allan variance for τ = 24 hours.

23. Electronic temperature compensation was used during this run. See the next section (Temperature Sensitivity of Output Frequency) for details.

24. NBS Time and Frequency Bulletin, No. 249, August 1978, p. 5

25. The temperature of the resonance cell is thermostatically controlled so that the resonance cell temperature coefficient is ~4 x $10^{-12}/^{o}C$ of ambient temperature.

26. Some of the factors that determine the stability of the pulse parameters are: temperature coefficients of the TTL integrated circuits and other timing circuits; voltage coefficients of the same circuits,

and the long-term stability and temperature coefficient of the voltage regulators for these circuits; long-term stability and temperature coefficients of the passive RC components used for timing in the timing circuits.

27. V. S. Zaks, Radio Eng. and Elect. Phys. 16, 1403 (1971).
28. All line widths in this report are the full widths at the points where the ordinate is equal to half of the peak value ("full width at half maximum").
29. T. C. English and J. C. Zorn, "Molecular Beam Spectroscopy," Chapter 6 in Methods of Experimental Physics, Vol 3, Molecular Physics, 2nd Edition, Part B, Dudley Williams, Editor (Academic Press, 1974), p. 760.
30. In the beam experiments, a molecule traveling through the apparatus passes through the rf (resonance) region. From its frame of reference, the molecule sees the rf as a pulse whose duration is equal to the time of flight through the rf region. The main difference between the beam case, and the gas cell case is the presence of relaxation for the gas cell atoms (for all practical purposes, molecules in the beam do not experience relaxation).
31. This is a description of the behavior to first order. Higher-order effects, which are small, are discussed in Appendix A.
32. W. Happer, Rev. Mod. Phys. 44, 169 (1972). See especially, pp. 196-198, 212.
33. M. Arditi and T. R. Carver, Phys. Rev. 136, A 643 (1964).
34. J. Vanier, Phys. Rev. 168, 129 (1968).
35. J. M. Andres, D. J. Farmer and G. T. Inouye, IRE Trans. Mil Elect., Vol. MIL-3, 178 (1959).
36. G. Missout and J. Vanier, Can. J. Phys. 53, 1030 (1975).
37. There is no advantage to improving the long-term stability of Rb devices to equal that of cesium and hydrogen devices if the size, weight and power consumption of Rb devices increases greatly (approaching that of cesium and hydrogen devices) in the process.
38. P. F. Panter, Modulation, Noise and Spectral Analysis (McGraw-Hill, 1965), p.p. 24-25.

APPENDIX A
THEORETICAL MODEL OF DEVICE OPERATION

In this appendix a theoretical model is developed that can be used to describe device operation. At the present time this model is restricted to the prediction of signal strengths as a function of device parameters, other than the frequency of the applied microwave radiation. That is, a theory of the line shape is not included at the present time.

This model begins with the fundamental quantum mechanical equations describing the optical pumping process, and subsequently incorporates characteristics of the present device.

Quantum Mechanics of Pulsed Optical Pumping

In this section we use a simplified version of the theory given by Vanier.[34] The theory, as developed in this section, applies to an optically thin layer of ^{87}Rb atoms within the resonance cell when the applied microwave field is resonant with the rubidium atoms. Our purpose here is to try to obtain closed-form analytical expressions that are subject to a simple physical interpretation without the necessity of using a computer. As it turns out, this can be done in a meaningful way that still allows us to relate the end product to the actual experimental situation.

We begin by assuming that the four assumptions stated on p. 129 of Vanier's paper are satisfied. While this is not strictly true in practice, the deviations from actual behavior due to these assumptions should be small. Vanier's theory treats the ^{87}Rb atom as a nine-level system: eight ground state sublevels and one optically excited state. Calculations[20] done using the full nine-levels indicate that it is a good approximation to consider the ground state as composed of only two levels, 1 and 2, corresponding respectively to ($F=1$, $M_F=0$) and ($F=2$, $M_F=0$). This results in an enormous mathematical simplification (8 x 8 matrices → 2 x 2 matrices). In fact, this three-level system is more like a two-level system because the excited state does not appear explicitly in the formalism.

Solution of Density Matrix Equations

Following Vanier's notation, the equations for the elements of the density matrix are, for a two-level ground state,

$$\dot{\rho} = -\tfrac{1}{2}\Gamma\rho - \gamma_1(\rho - \tfrac{1}{2}) - 2\beta\,\mathrm{Im}(\rho_{12}\,e^{-i\omega t}) \tag{A1}$$

$$\dot{\rho}_2 = \tfrac{1}{2}\Gamma\rho - \gamma_1(\rho_2 - \tfrac{1}{2}) + 2\beta\,\mathrm{Im}(\rho_{12}\,e^{-i\omega t}) \tag{A2}$$

$$\dot{\rho}_{12} = i\omega_o\rho_{12} - i\beta(\rho_2 - \rho)\,e^{i\omega t} +$$

$$-(\tfrac{1}{2}\Gamma + \gamma_2)\rho_2 - i\,\Delta\omega_\ell\,\rho_{12} \tag{A3}$$

where the dot indicates the partial derivative with respect to time; where the notation $\rho = \rho_{11}$, $\rho_2 = \rho_{22}$ has been used; where $T_1 = 1/\gamma_1$, and $T_2 = 1/\gamma_2$ are the time constants for the decay of the population difference and the oscillating magnetization, respectively; where Γ is the pumping rate due to the light; where $\omega_o/2\pi$ is the ^{87}Rb resonant frequency for the F=2, M_F=0 $\leftrightarrow$ F=1, M_F=0 hyperfine transition; where $\omega/2\pi$ is the frequency of the applied microwave radiation; and where $\Delta\omega_\ell/2\pi$ is the true light shift that is present only when the light is on, but is zero when the atoms are being interrogated by the microwave field. For pulsed pumping with optical detection by observing the absorption of the pumping light, the important quantity is $\rho(t)$. Since the pumping light and the applied microwave radiation are not present simultaneously, it suffices to solve the above equations for three special cases. This can easily be done using standard methods, plus the results given in Vanier's paper. In this way we obtain

$$\rho(t) = \tfrac{1}{2} + [\rho(0) - \tfrac{1}{2}]\,e^{-\gamma_1 t} \tag{A4}$$

$$\rho(t) = C + [\rho(0) - C]\,e^{-bt} \tag{A5}$$

$$\rho(t) = \tfrac{1}{2} - [\tfrac{1}{2} - \rho(0)]\, e^{-\gamma t} \cdot$$

$$\cdot (\cos st + \frac{\Delta\gamma}{2s} \sin st) \qquad \text{(A6)}$$

where

$$s \equiv \sqrt{(2\beta)^2 - (\Delta\gamma/2)^2} \qquad \text{(A7)}$$

$$C \equiv (2 + \Gamma/\gamma_1)^{-1} \qquad \text{(A8)}$$

$$b \equiv (\Gamma/2 + \gamma_1) \qquad \text{(A9)}$$

$$\gamma \equiv (\gamma_1 + \gamma_2)/2 \qquad \text{(A10)}$$

$$\Delta\gamma \equiv \gamma_2 - \gamma_1 \qquad \text{(A11)}$$

Eq. (A4) is for no light or microwave radiation present. Eq. (A5) is for light present, but no microwave. Eq. (A6) is for microwave present, but no light. In each case, $\rho(0)$ is the initial value of ρ for the conditions stated.

AM Signal

The quantity that is observed experimentally is the AM signal at resonance, denoted by S_{AM}. How this signal is generated is discussed in the section entitled, "AM Configuration". Here, we relate S_{AM} to $\rho(t)$.

The light absorption at time t is proportional to $\rho(t)$ and the intensity of the pumping light, so that

$$\text{absorption}(t) = k\Gamma\rho(t) \qquad \text{(A12)}$$

where k is a constant. The total light absorption during the duration of the light pulse is therefore equal to the integral of Eq. (A12) from 0 to T_ℓ. The average light absorption over one cycle of pulsing is therefore

$$\bar{a} \equiv \overline{\text{absorption}(t)} = (T_\ell + T_d)^{-1} \, kT \int_0^{T_\ell} \rho(t)\, dt \qquad \text{(A13)}$$

The observed signal is the difference between the values of $\bar{a}$ with the microwave on ($\beta \neq 0$) and off ($\beta = 0$), $s_{AM} = \bar{a}(\beta) - \bar{a}(0)$, where the lower case s indicates that this is the contribution to S_{AM} from an optically-thin layer of Rb atoms in the cell. It is convenient to write this as

$$s_{AM} = \Delta a^{AM} / (T_\ell + T_d) \qquad \text{(A14)}$$

$$\Delta a^{AM} = \frac{kT}{b} \cdot [\rho_a^{(\beta)} - \rho_a^{(0)}] \cdot (1 - e^{-bT_\ell}) \qquad \text{(A15)}$$

where $\rho_a^{(\beta)}$ is the initial value of ρ at the beginning of the light pulse, during that portion of the 10 Hz cycle when the microwave radiation is not gated off (light and microwave pulses alternated). Similarly, $\rho_a^{(0)}$ is the same quantity when the microwave radiation is gated off (light pulses only, and no microwave pulses). In effect, Δa^{AM} is the total change in the average absorption between microwave on and off with the duty cycle factor $(T_\ell + T_d)^{-1}$ removed. Finally, it should be noted that Eq. (A5) was used in Eq. (A13) to obtain Eqs. (A14) and (A15).

Steady-State Behavior

Figure A1 shows (schematically) the time behavior of ρ for one cycle of pulsing. In the treatment given here, T_s can be assumed to be zero without loss of generality.

In what follows, please keep in mind: that the population of the F=1 level is proportional to $\rho(t)$; that the value of ρ is ½ when the system is allowed to come to equilibrium in the dark with no microwave present; that the effect of the light is to produce a population inversion ($\rho<\frac{1}{2}$) by pumping atoms from the F=1 level to the F=2 level; that C is the value of ρ when the light has been present for a very long time with the microwave not present (i.e., C = value of ρ for cw lamp operation with microwave off). Under steady-state pulsing conditions we would expect behavior of the type shown in Figure A1: At the beginning of the light pulse, ρ has the value ρ_a, which is close to ½ (slight population inversion). The effect of the light is to pump atoms out of level 1 (F=1) to level 2 (F=2) so that the population of level 1 decreases exponentially in accordance with Eq. (A5) (with $\rho(0)$ replaced by ρ_a) toward the asymptotic (cw) value of C. At point b, $\rho = \rho_b$, the light goes off, and the microwave goes on. The net effect of the microwave is now to transfer atoms from level 2 to level 1. The population of level 1 therefore increases rapidly, according to Eq. (A6). At point c, $\rho = \rho_c$, and the microwave goes off leaving the atoms to slowly relax undisturbed in the dark. The population of level 1 during this portion of the pulsing cycle therefore asymptotically approaches the equilibrium value of ½, according to Eq. (A4). At the end of the pulsing cycle, $\rho = \rho_a'$. The condition for steady-state operation is that $\rho_a = \rho_a'$. Self consistency also requires that

$$\rho_b = \rho_I(T_\ell) = C + (\rho_a - C)\, e^{-bT_\ell} \tag{A16}$$

$$\rho_c = \rho_{II}(T_\mu) = \frac{1}{2} - \left(\frac{1}{2} - \rho_b\right) e^{-\gamma T_\mu} \cdot \left(\cos sT_\mu + \frac{\Delta\gamma}{2s} \sin sT_\mu\right) \tag{A17}$$

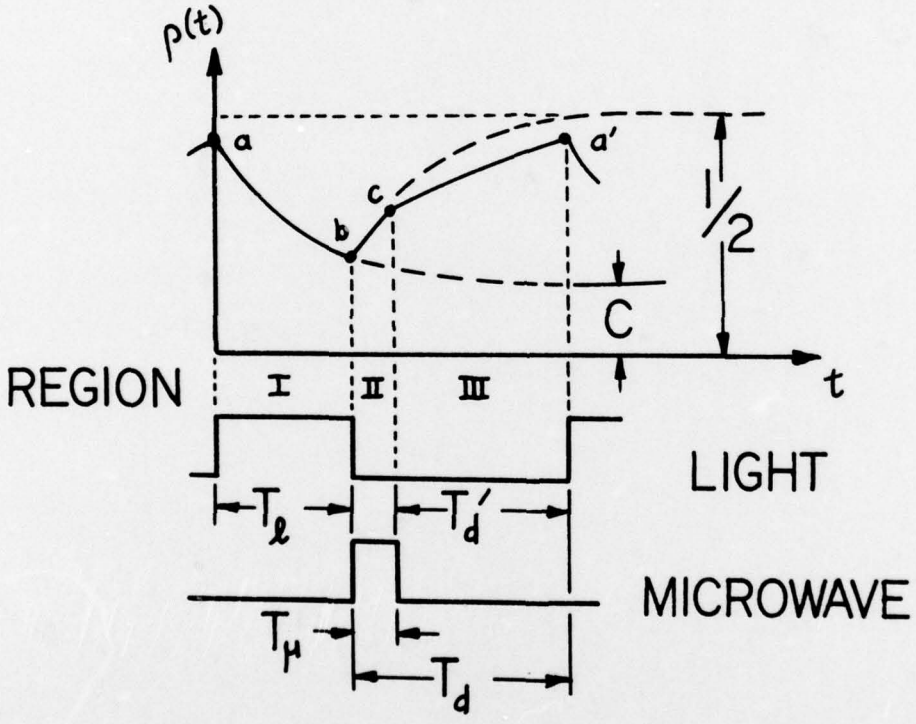

Figure A1. Schematic diagram of time dependence of $\rho(t)$ for steady state pulsing. Pulsing scheme is indicated at the bottom of the figure.

$$\rho_a = \rho_{III}(T_d') = \frac{1}{2} - \left(\frac{1}{2} - \rho_c\right) e^{-\gamma_1 T_d'} \tag{A18}$$

where we have used Eqs. (A5), (A6) and (A4) for ρ_I, ρ_{II}, ρ_{III}, respectively. Eqs. (A16), (A17) and (A18) constitute three equations in the three unknowns ρ_a, ρ_b, ρ_c in terms of (supposedly) known physical parameters. For our purposes, however, it suffices to solve only for ρ_a and to use the result in Eq. (A15). In fact, if Eq. (A15) is to be used, it is necessary to have two values of ρ_a. The first is $\rho_a^{(\beta)}$ which has already been discussed. The second is $\rho_a^{(0)}$ which can be obtained by solving for ρ_a in Eqs. (A16) to (A18) with $\beta = 0$ (and therefore, $s = i \cdot \Delta\gamma/2$, $T_\mu = 0$, and $T_d = T_d'$).

We have carried out this solution in the general case but the result is very complicated and not very illuminating. For this reason, we will now make one simplifying assumption, namely, that the lamp is pulsed on for a long enough time that ρ approaches the value for cw lamp operation (i.e., $\rho_b \tilde{=} C$). If this assumption is not made, then ρ_b becomes a complicated function of the device parameters and the initial condition for the period following the end of the light pulse depends on what happens during each part of the cycle.

Mathematically, the condition that $T_\ell \to \infty$ is equivalent to the above assumption. With this assumption, Eq. (A16) becomes $\rho_b = C$. If Eqs (A17), (A18) and the equation $\rho_b = C$ are now solved simultaneously for ρ_a, then both $\rho_a^{(\beta)}$ and $\rho_a^{(0)}$ can be obtained and the results substituted into Eq. (A15). If we denote Δa^{AM} as $T_\ell \to \infty$ by $\Delta\tilde{a}^{AM}$, then

$$\Delta\tilde{a}^{AM} \equiv \lim_{T_\ell \to \infty} \left(\Delta a^{AM}\right) \tag{A19}$$

$$\Delta\tilde{a}^{AM} = \frac{kT}{b}\left(\frac{1}{2} - C\right) e^{-\gamma_1 T_d} \cdot \left[1 - e^{-\frac{\Delta\gamma}{2} T_\mu}\left(\cos sT_\mu + \frac{\Delta\gamma}{2s} \sin sT_\mu\right)\right] \tag{A20}$$

Since $\beta \sim 1600\ \text{sec}^{-1}$ and $\Delta\gamma \sim 200\ \text{sec}^{-1}$ for our experimental apparatus, it is an excellent approximation to write $s = 2\beta$ and thus $\Delta\gamma/2s = \Delta\gamma/4\beta \sim 0.03$. This allows Eq. (A20) to be simplified.

$$\Delta\tilde{a}^{AM} = \frac{kT}{b}\left(\frac{1}{2} - C\right) e^{-\gamma_1 T_d} \cdot$$

$$\cdot \left[1 - e^{-\frac{\Delta\gamma}{2} T_\mu} \cos(2\beta T_\mu)\right] \qquad \text{(A21)}$$

Average over the Resonance Cell

Eq. (A21) is the contribution to the AM signal (aside from the duty cycle factor) from an optically-thin slice of the resonance cell (see Figure A2). It now remains to sum the contributions from all such slices. Before doing this, we note that the pumping rate is a function of z so that b and C are also functions of z according to Eqs. (A9) and (A8). We can therefore write

$$\Delta\tilde{A}^{AM} = \frac{1}{L}\int_0^L \Delta\tilde{a}^{AM}(z)\, dz \qquad \text{(A22)}$$

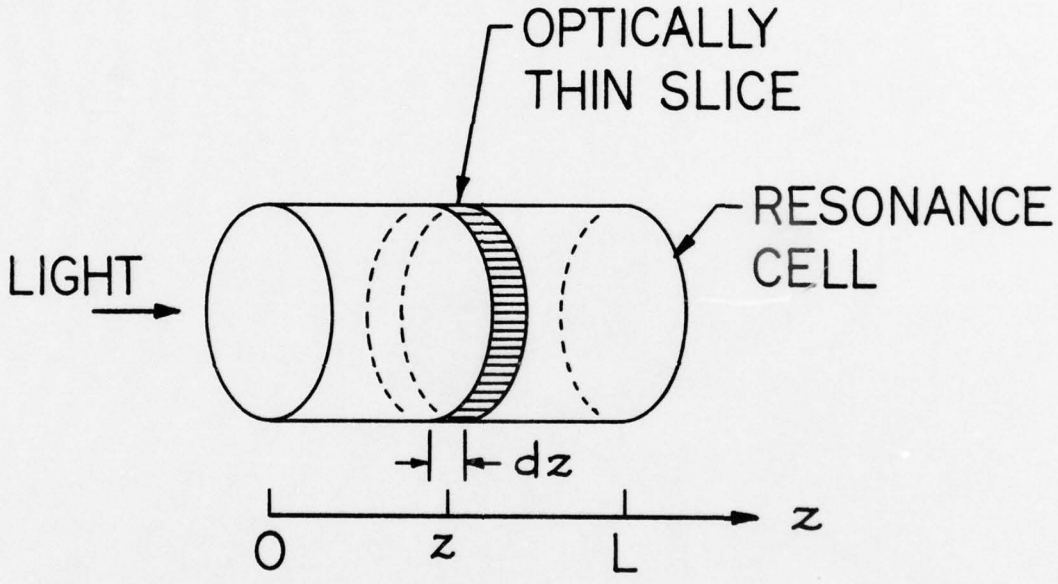

Figure A2. Schematic diagram of rubidium resonance cell (not to scale).

$$\Delta\tilde{A}^{AM} = \frac{1}{L} e^{-\gamma_1 T_d} \cdot$$

$$\cdot \int_0^L g(z) \left\{ 1 - e^{-\frac{\Delta\gamma}{2} T_\mu} \cos[2\beta(z) T_\mu] \right\} dz \qquad \text{(A23)}$$

$$\tilde{S}_{AM} = \Delta\tilde{A}^{AM} / (T_\ell + T_d) \qquad \text{(A24)}$$

$$g(z) \equiv \frac{k\Gamma(z)}{b(z)} \left[\frac{1}{2} - C(z) \right] \qquad \text{(A25)}$$

Before we can proceed further, we need to know the functional form of the pumping rate $\Gamma(z)$, and the microwave field parameter $\beta(z)$.

Since the resonance cell fills essentially the entire microwave cavity in our apparatus, the microwave field in the resonance cell is (to a first approximation) the same as in the cavity. Since the cavity operates in the TE_{111} mode, the z-component of microwave magnetic field is given by $H_z(z) = H_0 \sin(\pi z/L)$. We can therefore write

$$\beta(z) = \bar{\beta}_0 \sin(\pi z/L) \qquad \text{(A26)}$$

where $\bar{\beta}_0$ is an average value of β over the disk at the center of the cell.

The integral in Eq. (A23) still cannot be evaluated because $\Gamma(z)$ is unknown. Even if $\Gamma(z)$ were known, the resulting expression for $g(z)$ would probably be sufficiently complicated that the integral in Eq. (A23) could not be evaluated analytically. For this reason we consider two simple special cases, each of which contains some element of the truth.

Case (1): $g(z) = \text{constant} = g_0$

This case corresponds to a uniform optical pumping rate over the entire resonance cell. The integral in Eq. (A23) can now be evaluated in closed form. The result is

$$\Delta\tilde{A}^{AM} = g_0 e^{-\gamma_1 T_d} \left[1 - e^{-\frac{\Delta\gamma}{2} T_\mu} \cdot J_0(2\bar{\beta}_0 T_\mu)\right] \quad \text{(A27)}$$

where $J_0(x)$ is the zeroth order Bessel function with argument x.

Eq. (A27) has been plotted in Figure 18 as the dash-dot curve. The constants g_0 and $\bar{\beta}_0$ have been treated as adjustable parameters and their values chosen to give the best fit.

Case (2): $g(z)$ = step function

Figure A3 shows the form assumed for the excitation function $g(z)$, in this case. In the figure, g_1 is an adjustable constant. For this choice of $g(z)$, the rear of the cell is preferentially pumped by the light.[7] When this functional form of $g(z)$ is substituted into Eq. (A23), it is possible to evaluate analytically the integral. The result is an infinite series of Bessel functions of even order. In this case it is necessary to carry out numerical calculations through $J_{14}(x)$. This has been done and the results are presented in Figure 18 as the two dashed curves. (The two curves are for different values of the relaxation times.) Additional discussion of the results obtained here can be found in the main body of this report in the section entitled, "AM Signal as a Function of Pulse Parameters."

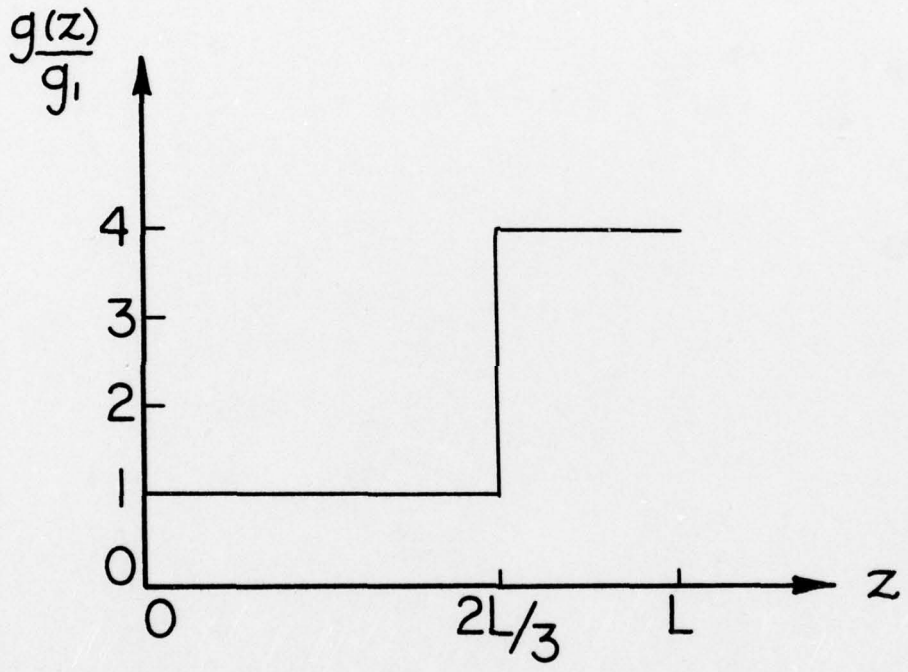

Figure A3. The step function g(z) over the length of the resonance cell, that is assumed for case (2). This is a measure of the optical pumping as a function of distance along the axis of the cell.